



ARTICLE

DOI: 10.1038/s41467-018-04250-4

OPEN

CO₂-sensitive tRNA modification associated with human mitochondrial disease

Huan Lin ¹, Kenryo Miyauchi¹, Tai Harada¹, Ryo Okita¹, Eri Takeshita^{2,3}, Hirofumi Komaki^{2,3}, Kaoru Fujioka⁴, Hideki Yagasaki⁴, Yu-ichi Goto^{2,3,5}, Kaori Yanaka⁶, Shinichi Nakagawa^{6,7}, Yuriko Sakaguchi¹ & Tsutomu Suzuki ¹

It has been generally thought that tRNA modifications are stable and static, and their frequencies are rarely regulated. N⁶-threonylcarbamoyladenine (t⁶A) occurs at position 37 of five mitochondrial (mt-)tRNA species. We show that YRDC and OSGEPL1 are responsible for t⁶A37 formation, utilizing L-threonine, ATP, and CO₂/bicarbonate as substrates. OSGEPL1-knockout cells exhibit respiratory defects and reduced mitochondrial translation. We find low level of t⁶A37 in mutant mt-tRNA isolated from the MERRF-like patient's cells, indicating that lack of t⁶A37 results in pathological consequences. Kinetic measurements of t⁶A37 formation reveal that the Km value of CO₂/bicarbonate is extremely high (31 mM), suggesting that CO₂/bicarbonate is a rate-limiting factor for t⁶A37 formation. Consistent with this, we observe a low frequency of t⁶A37 in mt-tRNAs isolated from human cells cultured without bicarbonate. These findings indicate that t⁶A37 is regulated by sensing intracellular CO₂/bicarbonate concentration, implying that mitochondrial translation is modulated in a codon-specific manner under physiological conditions.

¹Department of Chemistry and Biotechnology, Graduate School of Engineering, University of Tokyo, 7-3-1 Hongo, Bunkyo-ku, Tokyo 113-8656, Japan.

²Department of Mental Retardation and Birth Defect Research, National Institute of Neuroscience, National Center of Neurology and Psychiatry, 4-1-1 Ogawahigashi, Kodaira, Tokyo 187-8502, Japan. ³Department of Child Neurology, National Center Hospital, National Center of Neurology and Psychiatry, 4-1-1 Ogawahigashi, Kodaira, Tokyo 187-8502, Japan. ⁴Department of Pediatrics, Interdisciplinary Graduate School of Medicine and Engineering, University of Yamanashi, 1110 Shimokato, Chuo, Yamanashi, Yamanashi 409-3898, Japan. ⁵Medical Genome Center, National Center of Neurology and Psychiatry, 4-1-1 Ogawahigashi, Kodaira, Tokyo 187-8502, Japan. ⁶RNA Biology Laboratory, RIKEN Advanced Research Institute, 2-1 Hirosawa, Wako, Saitama 351-0198, Japan. ⁷RNA Biology Laboratory, Faculty of Pharmaceutical Sciences, Hokkaido University, Kita 12-jo Nishi 6-chome, Kita-ku, Sapporo 060-0812, Japan.

Correspondence and requests for materials should be addressed to T.S. (email: ts@chembio.t.u-tokyo.ac.jp)

Post-transcriptional modifications play diverse roles in RNA structure and function and are associated with various biological processes and physiological events^{1, 2}. To date, over 130 types of RNA modifications have been identified in various RNAs from all domains of life³. Transfer (t)RNAs contain multiple modifications involved in the stabilization of tRNA tertiary structure and precise decoding of genetic information^{4, 5}. A wide variety of RNA modifications are present in the anticodon regions of tRNAs, where they make critical contributions to the accuracy of protein synthesis at various steps of translation, including aminoacylation, decoding, and translocation. In particular, tRNA modifications at the first position of the anticodon (wobble position) modulate codon–anticodon interactions at the ribosomal A-site. Another hot spot in this region is a hypermodification at position 37, 3'-adjacent to the anticodon. These modifications strengthen codon–anticodon pairings by enhancing base-stacking interactions, thereby helping to maintain the correct reading frame during decoding. Optimal rate of translation fine-tuned by tRNA modifications supports correct folding of proteins, thereby maintaining proteome integrity⁶.

The mitochondrion is a eukaryotic organelle that generates ATP through respiration. In mammalian mitochondria, 22 species of tRNAs encoded in mitochondrial (mt)DNA play essential roles in the translation of 13 essential subunits of the respiratory chain complexes required for oxidative phosphorylation⁷. These mt-tRNAs are modified post-transcriptionally by nuclear-encoded tRNA-modifying enzymes. Loss of tRNA modifications or tRNA-modifying enzymes is strongly associated with human disease caused by mitochondrial dysfunction⁸. In previous work, among all species of bovine mt-tRNAs, we identified 15 types of RNA modification at 118 positions⁹. Two types of taurine-containing modifications, 5-taurinomethyluridine ($\tau\text{m}^5\text{U}$) and 5-taurinomethyl-2-thiouridine ($\tau\text{m}^5\text{s}^2\text{U}$), are mitochondria-specific modifications found at the wobble positions of mt-tRNAs responsible for two-codon sets ending in purines (NNR, R = A and G)¹⁰. We previously reported that $\tau\text{m}^5\text{U}34$ and $\tau\text{m}^5\text{s}^2\text{U}34$ are not formed in mutant mt-tRNAs^{Leu(UUR)} isolated from patients with MELAS (mitochondrial encephalopathy, lactic acidosis, and stroke-like syndrome)¹¹, or in mutant mt-tRNA^{Lys} isolated from patients with MERRF (myoclonus epilepsy with ragged-red fibers)¹². Lack of these taurine modifications results in defective mitochondrial translation, leading to pathological consequences related to mitochondrial dysfunction^{13, 14}. The pathogenic mutations in MELAS and MERRF are thought to act as negative determinants for the $\tau\text{m}^5\text{U}$ -modifying enzymes MTO1¹⁵ and GTPBP3¹⁶, and of the 2-thiouridylase MTU1^{17, 17}. Consistent with this idea, whole-exome sequencing identified loss-of-function mutations in each of these three genes in patients with mitochondrial disorders^{18–21}.

N^6 -threonylcarbamoyladenine (t^6A) (Fig. 1a) and its derivatives are universally conserved modifications found at position 37 of tRNAs responsible for codons starting with A (ANN codons)^{4, 22–26}. The bulky side chain of t^6A extends its planar ring via intramolecular hydrogen bonds and stabilizes the anticodon loop structure by strengthening π - π stacking with adjacent bases and preventing base pairing with U33²⁷. $\text{t}^6\text{A}37$ enhances tRNA binding to the A-site codon, as well as its efficient translocation²⁸, thereby helping to maintain the efficiency and accuracy of translation. $\text{t}^6\text{A}37$ also plays critical roles in aminoacylation of tRNA²⁹ and prevention of leaky scanning of initiation codons and read-through of stop codons³⁰. In mammalian mitochondria, $\text{t}^6\text{A}37$ is present in mt-tRNAs for Ser (AGY), Thr, Asn, Ile, and Lys (Fig. 1b)⁹. To date, however, the biogenesis and functional role of $\text{t}^6\text{A}37$ in mammalian mt-tRNAs have not been elucidated.

The biogenesis of t^6A has been well studied in bacterial systems. Formation of t^6A on tRNA was successfully reconstituted in vitro using four essential enzymes, YrdC (TsaC), YgjD (TsaD), YeaZ (TsaB), and YjeE (TsaE), in the presence of the substrates L-threonine (Thr), ATP, and $\text{CO}_2/\text{bicarbonate}$ ³¹. t^6A is formed in two consecutive reactions³². First, YrdC employs Thr, $\text{CO}_2/\text{bicarbonate}$, and ATP to synthesize threonylcarbamoyl-adenylate (TC-AMP), an active intermediate in t^6A formation. Next, the three other enzymes (YgjD, YeaZ, and YjeE) catalyze nucleophilic attack of the N^6 -amino group of A37 on the carbonyl carbon of TC-AMP to synthesize t^6A with release of AMP. YgjD is the catalytic subunit for t^6A formation, and YeaZ and YjeE serve as accessory proteins that facilitate YgjD to recognize diverse tRNAs and synthesize $\text{t}^6\text{A}37$. Structural studies revealed ATP-dependent assembly of the YgjD–YeaZ–YjeE complex³³. The yeast cytoplasm contains the YrdC/TsaC homolog Sua5p and an ancient protein complex called KEOPS, which consists of five subunits, Kae1, Bud32, Cgi121, Pcc1, and Gon7. The YgjD homolog Kae1 serves a catalytic function, with the assistance of the other four subunits, to regulate formation of t^6A in cytoplasmic tRNAs^{34–36}. Homozygous pathogenic mutation related to global developmental delay was found in *OSGEP* gene, a human homolog of *Kae1*³⁷. In addition, recessive mutations were found in four components of KEOPS complex in 32 families of Galloway–Mowat syndrome³⁸, indicating that hypomodification of t^6A in cytoplasmic tRNAs results in severe inherited disorders. On the other hand, in yeast mitochondria, the minimum enzyme system required for synthesis of $\text{t}^6\text{A}37$ in mt-tRNAs consists of only two components: Sua5p and Qri7p^{39, 40}. One isoform of Sua5p is localized to mitochondria and provides TC-AMP. Qri7p, a mitochondrial homolog of YgjD/Kae1, catalyzes $\text{t}^6\text{A}37$ formation utilizing TC-AMP generated by mitochondrial Sua5p. *Ara-bidopsis thaliana* GCPI1, a homolog of YgjD/Kae1, is localized to mitochondria, and is required for embryonic development in plants⁴¹.

YRDC and OSGEPL1 are human homologs of YrdC/Sua5 and YgjD/Qri7, respectively, and are predicted to be involved in $\text{t}^6\text{A}37$ formation in mt-tRNAs⁹. In vivo function of these homologs were confirmed by complementation of *Escherichia coli yrdC* and *ygdD* mutants³⁷. In this study, we demonstrated that YRDC and OSGEPL1 are responsible for $\text{t}^6\text{A}37$ formation in five species of mt-tRNAs. OSGEPL1 knockout cells exhibited respiratory defects and reduced mitochondrial translation, suggesting that $\text{t}^6\text{A}37$ plays a critical role in this process. We successfully reconstituted $\text{t}^6\text{A}37$ formation in mt-tRNAs with recombinant YRDC and OSGEPL1 in the presence of Thr, ATP, and bicarbonate. Kinetic studies revealed that bicarbonate concentration is the rate-limiting factor for $\text{t}^6\text{A}37$ formation in mitochondria. We observed hypomodification of $\text{t}^6\text{A}37$ in mt-tRNAs isolated from human cells cultured in the absence of CO_2 and bicarbonate, indicating that $\text{t}^6\text{A}37$ formation in mt-tRNAs is sensitive to intracellular bicarbonate concentration. We also identified several pathogenic mutations in mt-tRNA genes that impaired $\text{t}^6\text{A}37$ formation and confirmed that the level of $\text{t}^6\text{A}37$ was reduced in mt-tRNA^{Thr} bearing the A15923G mutation isolated from MERRF fibroblasts and myoblasts, indicating that the absence of $\text{t}^6\text{A}37$ has pathological consequences.

Results

Involvement of YRDC in $\text{t}^6\text{A}37$ formation in mitochondria.

YRDC (Uniprot: Q86U90) (Supplementary Fig. 1a), a human homolog of YrdC/Sua5, was supposed to catalyze TC-AMP formation. To examine the subcellular localization of human YRDC, we transiently expressed C-terminally FLAG-tagged YRDC in HeLa cells and detected the tagged protein by immunostaining.

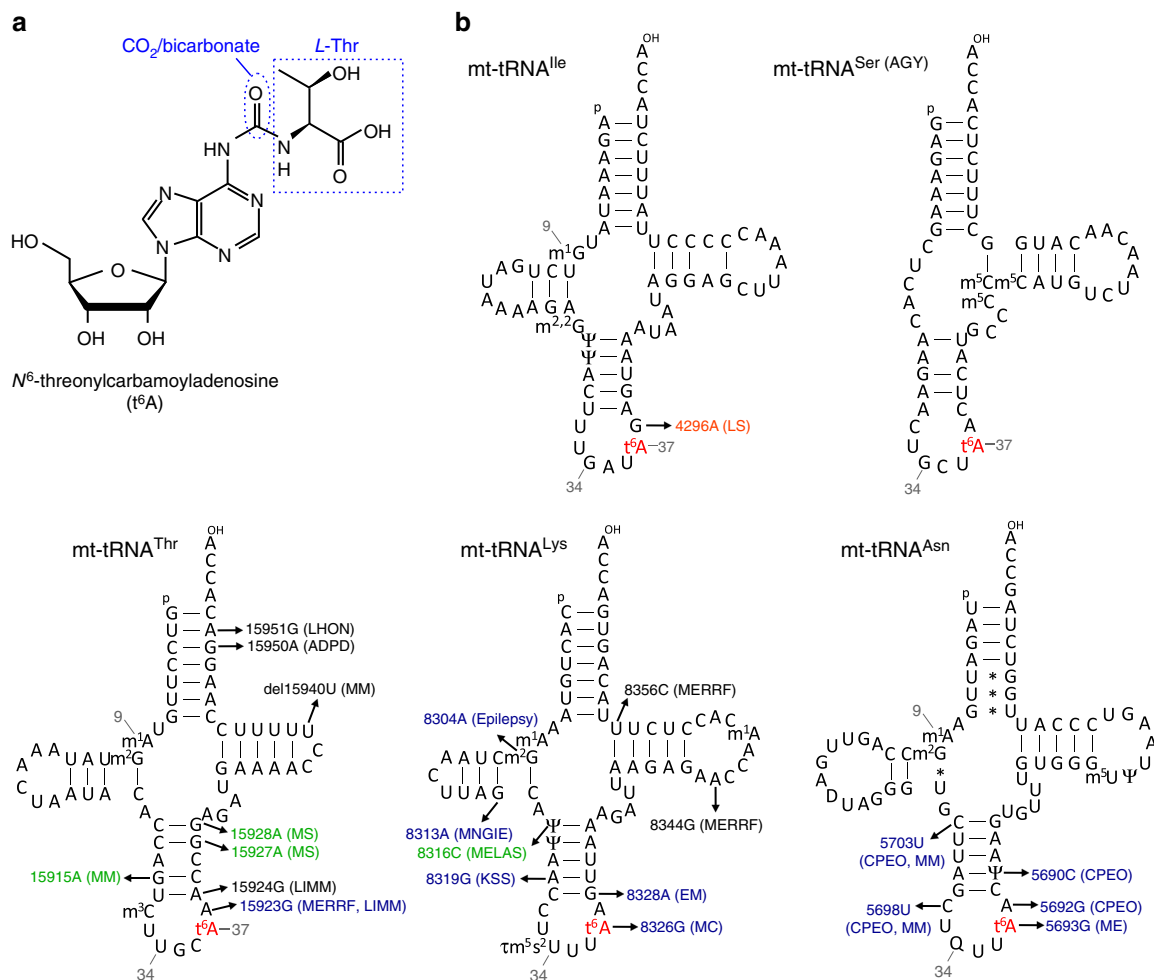


Fig. 1 N^6 -threonylcarbamoyladenine (t^6A) in human mt-tRNAs. **a** Chemical structure of t^6A . Carbonyl group derived from CO_2 /bicarbonate and Thr moiety are indicated. **b** Secondary structure and post-transcriptional modifications of five human mt-tRNAs bearing t^6A_{37} . Pathogenic point mutations deposited in MITOMAP⁷⁰ are indicated in each tRNA. The color codes for the mutations are consistent with those in Fig. 5c, d. Abbreviations: 1-methylguanosine, m^1G ; N^2,N^2 -dimethylguanosine, $m^{2,2}G$; pseudouridine, Ψ ; N^6 -threonylcarbamoyladenine, t^6A ; 5-methylcytidine, m^5C ; 1-methyladenine, m^1A ; N^2 -methylguanosine, m^2G ; 3-methylcytidine, m^3C ; 5-taurinomethyl-2-thiouridine, τm^5s^2U ; queuosine, Q; 5-methyluridine, m^5U ; LHON Leber hereditary optic neuropathy; ADPD Alzheimer's disease and Parkinson's disease; MM mitochondrial myopathy; MS multiple sclerosis; LIMM lethal infantile mitochondrial myopathy; MERRF myoclonus epilepsy associated with ragged red fibers; EM encephalomyopathy; KSS Kearns Sayre syndrome; MELAS mitochondrial myopathy, encephalopathy, lactic acidosis, and stroke-like episodes; MNGIE mitochondrial neurogastro intestinal encephalomyopathy; CPEO chronic progressive external ophthalmoplegia; MC mitochondrial cytopathy; LS Leigh syndrome

As shown in Fig. 2a, YRDC was widely diffused throughout the cell, but tended to be more strongly localized to the cytoplasm. As determined by WoLF PSORT⁴², a tool for predicting protein localization, YRDC has an N-terminal mitochondrial targeting sequence (MTS) (Supplementary Fig. 1a and Fig. 2c), implying mitochondrial localization. To confirm this prediction, we isolated the mitochondrial fraction from HEK293T cells expressing YRDC-FLAG and performed western blotting alongside whole-cell lysate as a control. The purity of the mitochondrial fraction was confirmed by the absence of GAPDH signal (a cytoplasmic marker) and a strong CO1 signal (cytochrome c oxidase subunit I) (Fig. 2b). We clearly detected YRDC-FLAG in the mitochondrial fraction (Fig. 2b). In cells expressing an YRDC-FLAG variant with an N-terminal truncation ($\Delta 2-15$), very little signal was detected in the mitochondrial fraction, although it was detected in whole-cell lysate (Fig. 2b). We then constructed two YRDC-FLAG variants with MTS mutations, S17F and A15F/S17F, both of which improve PSORT scores for mitochondrial localization. For both variants, clear signals were observed in mitochondrial

regions (Fig. 2a), indicating that the MTS mutations promoted mitochondrial localization of YRDC-FLAG. Consistent with this, western blotting (Fig. 2b) showed a strong signal in the mitochondrial fraction corresponding to the A15F/S17F variant. Because YRDC has a weak MTS, a large fraction of YRDC localizes in the cytoplasm and participates in t^6A_{37} formation in cytoplasmic tRNAs, whereas a smaller fraction of YRDC is imported to mitochondria where it performs the same function for mitochondrial tRNAs. The MTS is frequently cleaved by mitochondrial processing protease after import⁴³. To determine the cleavage sites in the MTS, we immunoprecipitated YRDC-FLAG and subjected the precipitated protein to mass-spectrometric analysis. We detected seven tryptic peptides derived from the N-terminus of YRDC (Fig. 2c and Supplementary Fig. 2a, b), indicating that multiple cleavages took place in mitochondria. Each peptide was sequenced by collision-induced dissociation (CID) to identify its N-terminus (Fig. 2c and Supplementary Fig. 2c), revealing six long isoforms with cleavage sites at positions 13–18 and one short isoform with the cleavage

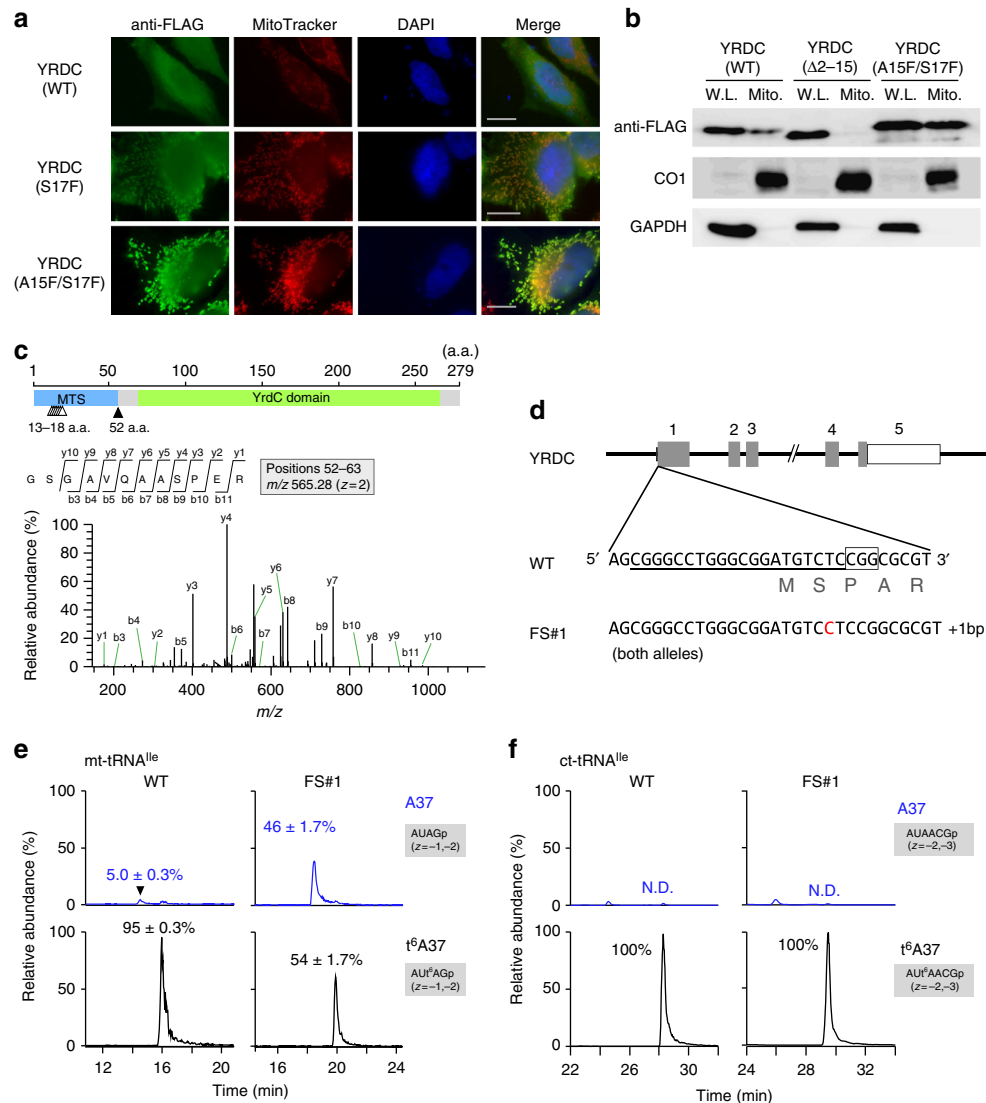


Fig. 2 YRDC is responsible for t^6A37 formation in mt-tRNAs. **a** Subcellular localization of wild-type (WT) and mutant YRDC (S17F, A15F/S17F) in HeLa cells immunostained with an anti-FLAG antibody (Green). Nuclei and mitochondria were stained with DAPI (blue) and MitoTracker (Red), respectively. All images were superimposed to generate the merged panel. Scale bars: 20 μ m. **b** Mitochondrial localization of YRDC. Whole-cell lysates (W.L.) and mitochondrial fractions (Mito.) from HEK293T cells transfected with WT, variant with N-terminal truncation (a.a. Δ 2–15), and mutant (A15F/S17F) YRDC constructs were subjected to western blotting with anti-FLAG antibody to detect YRDC variants, anti-CO1 (mitochondrial marker), and anti-GAPDH (cytoplasmic marker). Uncut gel images are provided in Supplementary Fig. 15. **c** Determination of the cleavage site in the MTS of YRDC. Schematic depiction of YRDC with a predicted MTS (blue) and a conserved region homologous to that of *E. coli* YrdC (green). Multiple cleavage sites in the long and the short isoforms of YRDC expressed in HeLa cells are indicated by white and black arrowheads, respectively. The CID spectrum represents the sequence of the N-terminal tryptic peptide of the short isoform with the cleavage site at position 52. The precursor ion for CID is m/z 565.28. Product ions are assigned on the peptide sequence. **d** Top: schematic of human YRDC gene and the site of insertion introduced with the CRISPR-Cas9 system. Shaded boxes indicate coding regions; open boxes indicate untranslated regions of exons; lines indicate introns. Inset: exon 1 of WT YRDC. The target sequence of the single guide RNA (sgRNA) is underlined; the protospacer adjacent motif (PAM) sequence is outlined. Bottom: sequence of the frameshift cell line (FS#1); the inserted C is indicated in red. **e** Extracted ion chromatograms (XICs) generated by integration of multiply-charged negative ions of the A37-containing fragments of human mt-tRNA^{le} with A37 (top) or t^6A37 (bottom) (Supplementary Table 1) isolated from WT (left) and FS#1 (right) cell lines. t^6A frequencies (%) are described as mean values \pm s.d. of technical triplicate. **f** XICs generated by integration of multiply-charged negative ions of A37-containing fragments of human ct-tRNA^{le(IAU)} with A37 (top) or t^6A37 (bottom) (Supplementary Table 1) isolated from WT (left) and FS#1 (right) cell lines

site at position 52 (Supplementary Fig. 1a, 2a). The existence of these truncated forms of YRDC supports our conclusion that a subset of YRDC is imported into mitochondria.

To confirm that YRDC is involved in mitochondrial t^6A formation, we tried to knock out YRDC in HEK293T cells using the CRISPR/Cas9 system. However, we failed to obtain a null allele, indicating that YRDC is essential for cell viability. Next, we

re-designed the single guide RNA (sgRNA) to target the N-terminus of YRDC, with the hope of obtaining cell lines harboring a mutation in the MTS (Fig. 2d). In this manner, we obtained a cell line, FS#1, in which one nucleotide was inserted at the second codon of YRDC in both alleles (Fig. 2d). We then used reciprocal circulating chromatography to isolate both mitochondrial and cytoplasmic (ct-)tRNAs^{le} from FS#1⁴⁴ and analyzed the

status of t⁶A37 by capillary LC-nano-ESI-mass spectrometry (RNA-MS)⁴⁵. As shown in Fig. 2e, we detected RNase T₁-digested fragments with t⁶A37 or A37 for both tRNAs (Supplementary Table 1) isolated from WT and FS#1 cells. To estimate ESI detection efficiencies of RNA fragments with and without t⁶A modification, we performed calibration curves for RNase T₁-digested fragments of human mt-tRNA^{Leu} with varying t⁶A frequency (Supplementary Fig. 3). The regression line with a slope of 1 exhibited $r^2 = 0.9913$, suggesting that t⁶A does not affect largely on ESI detection efficiency of RNA fragments. Thus, we can relatively quantify t⁶A frequency from their intensities of mass chromatograms.

In mt-tRNA^{Leu}, the t⁶A37 frequency in WT cells (95%) was clearly reduced to 54% in FS#1 cells; consistent with this, a large fraction (46%) of hypomodified mt-tRNA^{Leu} was detected in FS#1 cells. By contrast, no reduction of t⁶A37 frequency was observed in ct-tRNA^{Leu} from FS#1 (Fig. 2f), indicating that the +1 frameshift mutation partially impaired mitochondrial localization of YRDC. Given that cytoplasmic t⁶A was not impaired in FS#1 cells, we hypothesize that Met at position 10 of YRDC (Supplementary Fig. 1a) functions as an alternative initiation site for production of cytoplasmic YRDC in this cell line. Otherwise, if mitochondrial localization of YRDC is completely impaired by the +1 frameshift mutation, TC-AMP produced by cytoplasmic YRDC might be imported to mitochondria by penetrating mitochondrial membranes, and used for mitochondrial t⁶A37 formation.

OSGEPL1 is involved in t⁶A37 formation in mitochondria.

OSGEPL1 (Uniprot: Q9H4B0) (Supplementary Fig. 1b), a human homolog of Ygd/Qri7, is predicted to be involved in t⁶A37 formation in mitochondria⁹. To explore this possibility, we examined the subcellular localization of C-terminally FLAG-tagged OSGEPL1 transiently expressed in HeLa cells. As shown in Fig. 3a, OSGEPL1 was predominantly localized in mitochondria. Consistent with this, iPSORT analysis⁴⁶ predicted the existence of an MTS in the N-terminal region (positions 1–33) of OSGEPL1 (Supplementary Fig. 1b). The OSGEPL1 variant with the MTS truncation ($\Delta 2-33$) did not translocate to mitochondria, but was instead diffused throughout the cytoplasm (Fig. 3a). To determine the cleavage site in the MTS, we immunoprecipitated OSGEPL1-FLAG expressed in HEK293T cells and subjected the precipitated protein to MS. We detected an N-terminal peptide starting at position 35 (Fig. 3b and Supplementary Fig. 1b), indicating that a 34-a.a. N-terminal peptide was removed in mitochondria. This finding is consistent with the previous report that endogenous OSGEPL1 was detected in mitochondrial fraction of HeLa cells by cross-reactivity of *A. thaliana* anti-GCP1 antibody⁴¹.

Next, we knocked out OSGEPL1 in HEK293T cells using the CRISPR/Cas9 system and obtained two cell lines (KO#1 and KO#2) with frameshift mutations in both alleles (Fig. 3c). No endogenous OSGEPL1 was detected in either cell line by western blotting (Fig. 3d). Next, we isolated five species of mt-tRNAs containing t⁶A37, along with ct-tRNA^{Leu} as a control, from WT cells and the two KO lines, digested each tRNA with RNase T₁, and subjected the digested products to RNA-MS. We detected RNase T₁-digested fragments containing t⁶A37 (Supplementary Table 1) from all tRNA species isolated from WT cells. Judging from the ratio of modified (t⁶A37) versus unmodified (A37) fragments, more than 62% (62–97%) of tRNAs contained the t⁶A37 modification (Fig. 3e and Supplementary Fig. 4). In all five species of mt-tRNAs isolated from OSGEPL1-KO cells, t⁶A37 was completely absent and converted to unmodified A37 (Fig. 3e and Supplementary Fig. 4). On the other hand, as expected based on the involvement of the KEOPS complex in cytoplasmic t⁶A

formation, the t⁶A37 frequency was not altered in ct-tRNA^{Leu} isolated from the KO cells (Fig. 3f). These results demonstrated that OSGEPL1 is exclusively involved in t⁶A37 formation in mitochondria.

During RNA-MS analysis of mt-tRNA^{Thr} (Fig. 1b) isolated from the OSGEPL1-KO cells, we detected hypomodification of 3-methylcytidine (m³C) at position 32 (Supplementary Table 1). The high m³C frequency (94%) in WT cells was reduced to 67% in KO#1 and to 64% in KO#2 (Supplementary Fig. 5a), suggesting that t⁶A37 is required for efficient m³C32 formation.

When OSGEPL1-KO cells were rescued by plasmid-encoded OSGEPL1, t⁶A37 levels were partially restored (Fig. 3e). By contrast, t⁶A37 was not rescued by MTS-truncated OSGEPL1 (a.a. $\Delta 2-33$) (Fig. 3e), suggesting that mitochondrial localization mediated by the MTS is essential for t⁶A37 formation in mt-tRNAs.

Loss of OSGEPL1 causes mitochondrial dysfunction.

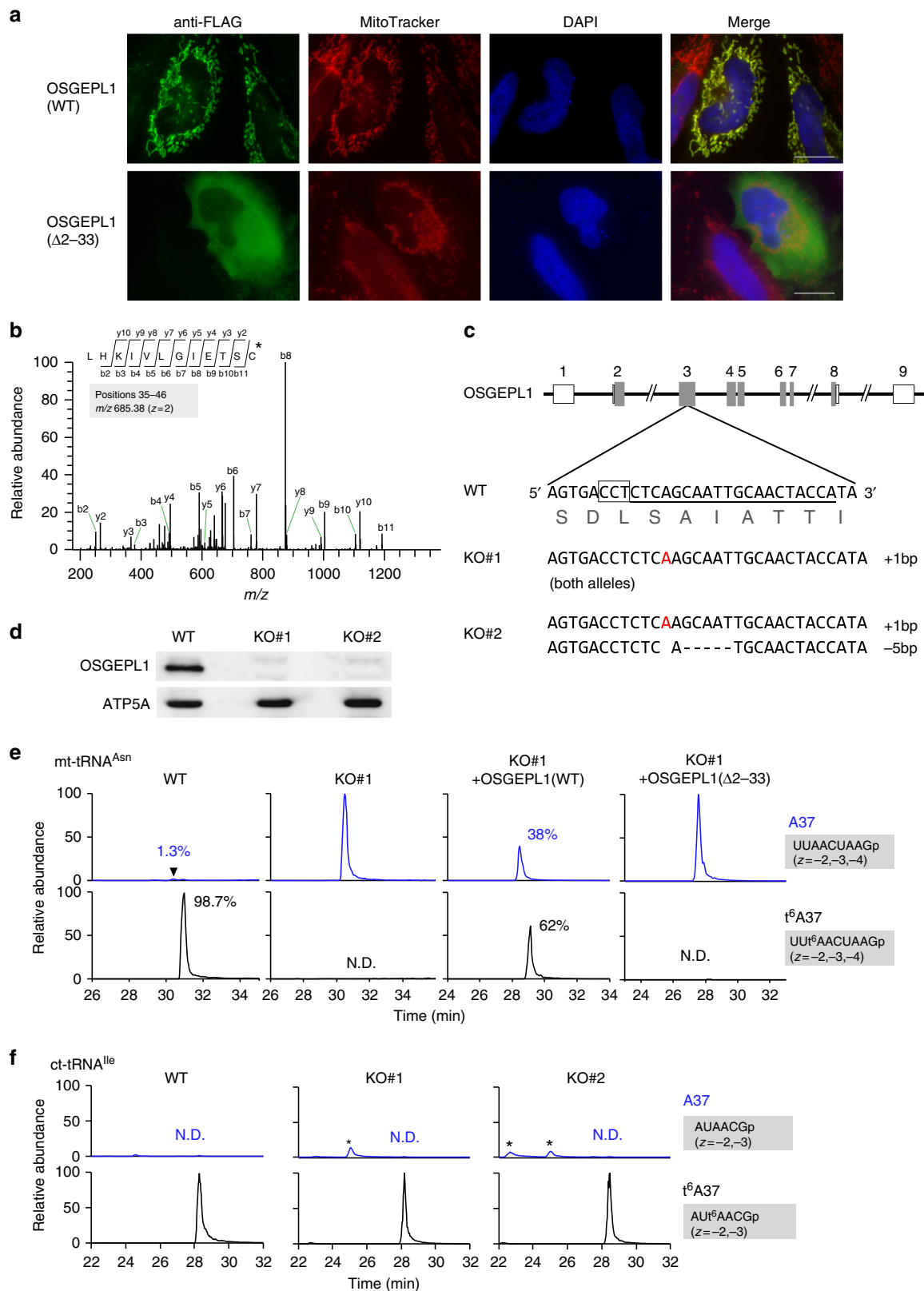
Next, we assessed mitochondrial activity of OSGEPL1-KO cells by monitoring cell growth in medium containing galactose, a non-fermentable sugar, as the primary carbon source⁴⁷. OSGEPL1-KO cells grew slightly slower than WT cells in glucose medium (Fig. 4a), but exhibited a severe growth defect in galactose medium (Fig. 4a), indicating mitochondrial dysfunction in OSGEPL1-KO cells. Measurement of respiratory activity and ATP levels in OSGEPL1-KO cells revealed that the oxygen consumption rate (OCR) (Fig. 4b) and ATP level (Fig. 4c) in KO cells were significantly lower than those in WT cells. To explore this phenomenon in greater details, we biochemically compared respiratory complex activities between OSGEPL1-KO and WT cells (Fig. 4d). We observed a clear reduction in Complex I, whereas no significant change was observed in other complexes. Consistent with this, the steady-state levels of ND2 and ND5, both of which are subunits of Complex I were markedly reduced in OSGEPL1-KO cells (Fig. 4e and Supplementary Fig. 6a). We also observed a slight reduction in the level of NDUFB8, a nuclear-encoded complex I subunit, indicating that assembly of Complex I was impaired in OSGEPL1-KO cells. To examine mitochondrial translational activity, we carried out a pulse-labeling experiment (Fig. 4f and Supplementary Fig. 6b). Specifically, we treated OSGEPL1-KO and WT cells with emetine to inhibit cytoplasmic translation and then added [³⁵S] methionine and [³⁵S] cysteine to the medium to specifically label mitochondrial translational products. Mitochondrial protein synthesis was clearly lower in OSGEPL1-KO cells than in WT cells (Fig. 4f). In particular, the levels of subunits of Complex I, including ND1, ND2, ND4, ND5, and ND6, were markedly reduced. Given that t⁶A37 has pleiotropic functions in protein synthesis, this result can be attributed to the hypomodification of mt-tRNAs in OSGEPL1-KO cells.

t⁶A37 is required for efficient aminoacylation in bacterial tRNAs²⁹. Accordingly, we next measured the aminoacylation levels in mt-tRNA^{Lys} by acid-urea northern blotting (Fig. 4g). In WT cells, mt-tRNA^{Lys} was fully lysylated, whereas we clearly detected deacylated mt-tRNA^{Lys} in OSGEPL1-KO cells. Based on band intensities, the aminoacylation levels of mt-tRNA^{Lys} were 98.4% in WT, 89.9% in KO#1, and 83.9% in KO#2. As an important control, we observed no alteration of aminoacyl-mt-tRNA^{Val}, which has no t⁶A37, in OSGEPL1-KO cells. This finding demonstrated that t⁶A37 is required for efficient aminoacylation of mt-tRNA^{Lys} in human mitochondria. To determine the steady-state level of the five mt-tRNAs in OSGEPL1-KO cells, we carried out northern blotting, but found no significant alteration in the levels of any of these tRNAs (Supplementary Fig. 7), indicating that lack of t⁶A37 has little effect on tRNA stability.

In vitro reconstitution of mitochondrial t⁶A37 formation. In general, most tRNAs from all domains of life have highly conserved intramolecular tertiary interactions, including the D-loop/T-loop ‘kissing’ interaction that promotes folding into the L-shaped tertiary structure. However, most mammalian mt-tRNAs lack such D-loop/T-loop interactions and instead adopt non-

canonical cloverleaf structures⁷. In fact, the sizes and sequences of the D/T-loops in t⁶A-containing mt-tRNAs vary considerably (Fig. 1b). In particular, mt-tRNA^{Ser(AGY)} lacks the entire D-arm.

To determine how OSGEPL1 recognizes these mt-tRNAs with diverse structures, we established an in vitro reconstitution system for mitochondrial t⁶A formation and examined its



substrate specificity. Soluble YRDC and OSGEPL1 were recombinantly expressed in *E. coli*. As tRNA substrates, we prepared five species of human mt-tRNAs for Thr, Asn, Ile, Ser(AGY), and Lys by in vitro transcription. These tRNAs were incubated with recombinant YRDC (17–279a.a.) and OSGEPL1 (35–414a.a.) in the presence of Thr, ATP, and bicarbonate. The products were digested by RNase T₁ and subjected to RNA-MS. We detected t⁶A-containing fragments only in the presence of both enzymes (Fig. 5a, b and Supplementary Fig. 8a, b). t⁶A37 was efficiently introduced into mt-tRNAs for Thr (96%) (Fig. 5a), Asn (98%), and Lys (95%) (Supplementary Fig. 8a). By contrast, efficiency of t⁶A37 formation was lower in the mt-tRNAs for Ile (67%) (Fig. 5b) and Ser(AGY) (34%) (Supplementary Fig. 8b). We considered that this outcome might be due to the lack of other modifications in tRNA transcripts. Accordingly, we isolated individual mt-tRNA^{Ile} and mt-tRNA^{Ser(AGY)} lacking t⁶A37 from OSGEPL1-KO cells and examined t⁶A37 formation in these tRNAs in vitro. The frequency of t⁶A37 formation was markedly increased (from 67 to 93%) in mt-tRNA^{Ile} (Fig. 5b), but slightly increased (from 34 to 48%) in mt-tRNA^{Ser(AGY)} (Supplementary Fig. 8b). This result suggests that modifications in other regions contribute to the efficiency of t⁶A37 formation in these mt-tRNAs.

To characterize mitochondrial t⁶A37 formation, we examined the activity of *E. coli* t⁶A-modifying enzymes (YrdC, YgjD, YjeE, and YeaZ) toward the five mt-tRNAs under the same assay conditions. The *E. coli* system introduced t⁶A37 efficiently in mt-tRNAs for Thr (93%), Asn (94%), and Lys (90%) (Supplementary Fig. 8c), but much less efficiently in mt-tRNAs for Ile (6%) and Ser(AGY) (7%) (Supplementary Fig. 8c), indicating that the *E. coli* system has substrate specificity for t⁶A37 formation. Together, these findings indicate that human OSGEPL1 evolved to acquire broad substrate specificity to accommodate at least five mt-tRNAs with diverse structures.

We found several isoforms of YRDC with different N-termini. To compare their activities, we prepared three YRDC isoforms (full length, 17–279a.a. and 52–279a.a.) (Fig. 2c), and compared their t⁶A-forming activity using mt-tRNA^{Asn} as a substrate. They all showed efficient activity with little significant difference between three isoforms (Supplementary Fig. 9).

Pathogenic mutations impair mitochondrial t⁶A37 formation.

Pathogenic mutations in mtDNA are associated with mitochondrial disorders (MITOMAP: <http://mitomap.org/MITOMAP>). Among them, about 200 mutations reside in tRNA genes. Curiously, pathogenic mutations in each tRNA are linked to different symptoms of mitochondrial diseases. Given that t⁶A37 plays critical roles in mitochondrial protein synthesis, we speculated that some of the pathogenic point mutations in mt-tRNA genes

impair t⁶A37 formation, in turn leading to mitochondrial dysfunction. From among the previously described pathogenic mutations, we prepared 21 mutant mt-tRNAs for Thr, Lys, and Asn (Fig. 1b) by in vitro transcription and then examined their ability to undergo t⁶A37 modification mediated by YRDC and OSGEPL1 (Fig. 5c). As expected, two of the target-site mutations, A8326G in mt-tRNA^{Lys} and A5693G in mt-tRNA^{Asn}, completely abolished t⁶A37 formation. Among eight mutants of mt-tRNA^{Thr}, only A15923G strongly inhibited t⁶A37 formation, whereas three mutations, G15915A, G15927A, and G15928A, had a milder effect with relative activity 0.4–0.8. In mt-tRNA^{Lys}, four mutations (G8304A, G8313A, A8319G, and G8328A) caused severe reductions in t⁶A37 formation with relative activity less than 0.3. In mt-tRNA^{Asn}, t⁶A37 formation was markedly impaired by four mutations (C5703U, C5698U, A5692G, and U5690C) with relative activity less than 0.3. Collectively, among 21 pathogenic point mutations in three mt-tRNA genes, two target-site mutations and nine mutations strongly affected t⁶A37 formation, indicating that loss of t⁶A37 is a major cause of mitochondrial disorders. Multiple mutations that reduced t⁶A37 reside in the anticodon arm of mt-tRNAs (Fig. 1b), suggesting that OSGEPL1 primarily recognizes the anticodon step-loop structure to introduce t⁶A37.

Because we detected little t⁶A37 formation in mt-tRNA^{Thr} bearing the A15923G mutation, as well as in mt-tRNA^{Asn} bearing the A5692G mutation (Fig. 5c), we concluded that A38 is a strong determinant for t⁶A37 formation and that A-to-G mutation in this position strongly impaired t⁶A37 formation. Nevertheless, human mt-tRNA^{Ile} contains G38 (Fig. 1b), explaining why mt-tRNA^{Ile} is a poor substrate for OSGEPL1 as observed in Fig. 5b. Notably in this regard, a G-to-A pathogenic mutation at position 38 (G4296A) is associated with Leigh syndrome (Figs. 1b and 5d)⁴⁸. We prepared in vitro transcripts of mt-tRNA^{Ile} bearing the G4296A mutation and examined its ability to undergo t⁶A37 formation. The G4296A mutation significantly promoted t⁶A37 formation (Fig. 5d), suggesting that the G38 residue in WT mt-tRNA^{Ile} plays a regulatory role in preventing t⁶A37 formation.

Hypomodification of t⁶A37 in mt-tRNA in patient cells. To verify the loss of t⁶A37 in mutant mt-tRNAs in patient cells, we obtained fibroblasts and myoblasts harboring the A15923G mutation from a 12-year-old female patient with symptoms of MERRF, lactic acidosis, short stature, and hearing loss. Because clinical specimens are heteroplasmic with respect to mtDNA, we first determined the mtDNA mutation rate using the restriction fragment length polymorphism (RFLP) method (Supplementary Fig. 10a)). The A15923G mutation rate in fibroblasts and myoblasts was 32% and 62%, respectively (Supplementary Fig. 10b). We then isolated mt-tRNA^{Thr}, along with mt-tRNA^{Ser(AGY)} and

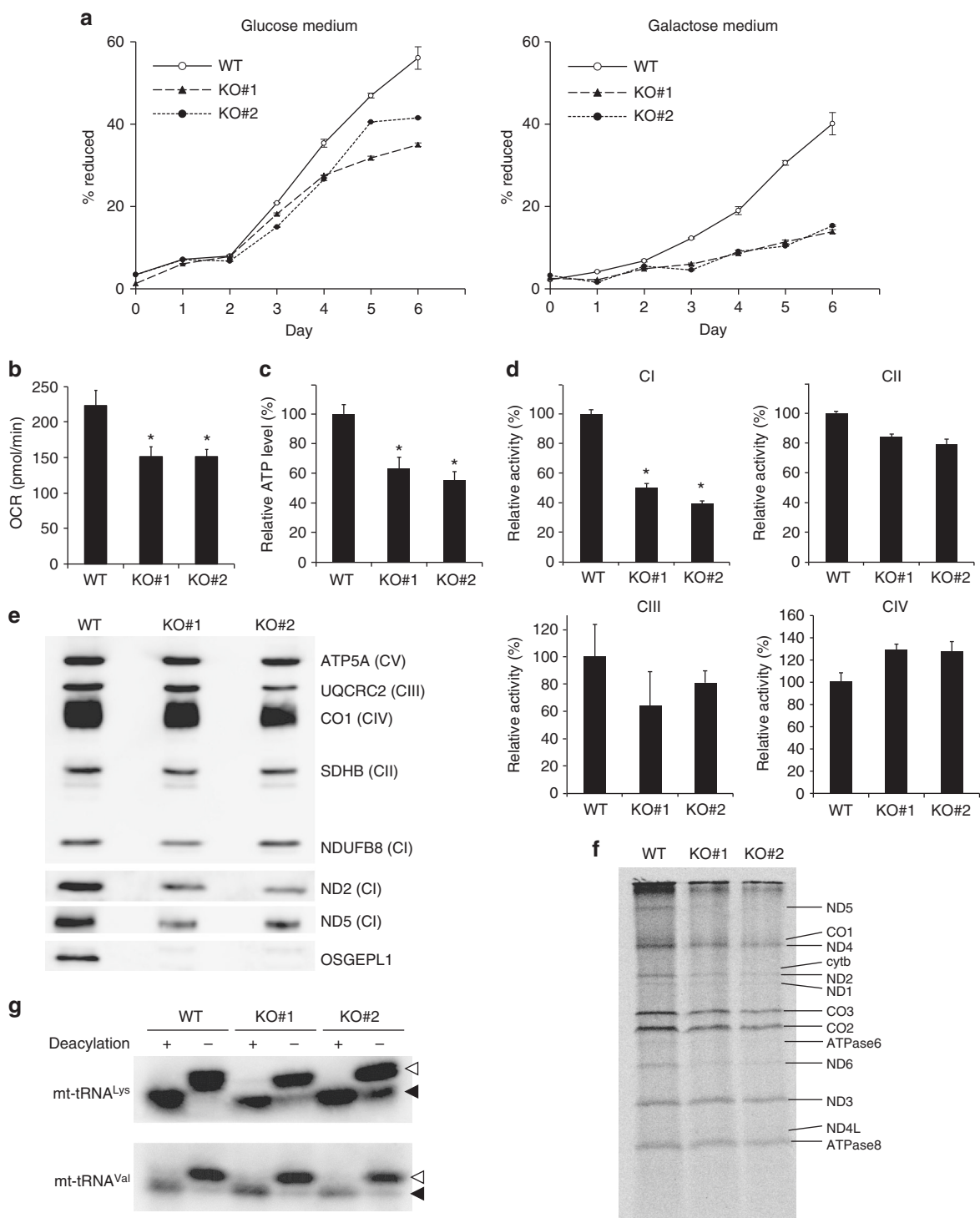
Fig. 3 OSGEPL1 is responsible for t⁶A37 formation in mt-tRNAs. **a** Subcellular localization of wild-type (WT) and N-terminal truncated (a.a. Δ2–33) OSGEPL1 in HeLa cells immunostained with an anti-FLAG antibody (Green). Nuclei and mitochondria were stained with DAPI (blue) and MitoTracker (Red), respectively. All images were superimposed to generate the merged panel. Scale bars: 20 μm. **b** Determination of the cleavage site in the MTS in OSGEPL1. The CID spectrum represents a sequence of N-terminal peptide of OSGEPL1 starting from position 35. The precursor ion for CID is *m/z* 685.38. Product ions are assigned on the peptide sequence. C* stands for alkylated cysteine residue. **c** Top: schematic of human OSGEPL1 gene and sites of mutations introduced by the CRISPR-Cas9 system. Shaded boxes indicate coding regions; open boxes indicate untranslated regions of exons; lines indicate introns. Inset: exon 3 of WT OSGEPL1. The target sequence of the single guide RNA (sgRNA) is underlined; the protospacer adjacent motif (PAM) sequence is outlined. Bottom: sequences of KO#1 and KO#2 cell lines. The inserted sequence is indicated in red and deleted sequences are indicated by dashed lines. **d** Confirmation of KO lines by western blotting of endogenous OSGEPL1 and the mitochondrial marker ATP5A (as a control). Uncut gel images are provided in Supplementary Fig. 15. **e** XICs generated by integration of multiply-charged negative ions of the A37-containing fragments of human mt-tRNA^{Asn} bearing A37 (top) or t⁶A37 (bottom) (Supplementary Table 1) isolated from WT, KO#1, and KO#1 rescued by plasmid-encoded OSGEPL1 (WT and a.a. Δ2–33). N.D., not detected. Intensity fractions (%) of modified or unmodified fragments are indicated. **f** XICs generated by integration of multiply-charged negative ions of the A37-containing fragments of human ct-tRNA^{Ile(IAU)} bearing A37 (top) and t⁶A37 (bottom) (Supplementary Table 1) isolated from WT, KO#1, and KO#2

ct-tRNA^{Ile}(IAU), from the mutant cells. Because the isolated mt-tRNA^{Thr} contained a mixture of WT and A15923G mutant tRNAs, we analyzed these two tRNAs separately by digesting with two different RNases. For WT mt-tRNA^{Thr}, we detected a t⁶A37-containing heptamer fragment (positions 36–42) generated by RNase T₁ digestion (Fig. 5e). For mt-tRNA^{Thr} harboring the A15923G mutation we used RNase A to detect tetramer fragments (positions 37–40) to measure t⁶A37 frequency (Fig. 5e). We observed low levels of t⁶A37 in myoblasts (6%) (Fig. 5e) and fibroblasts (5%) (Supplementary Fig. 10c), whereas WT mt-tRNA^{Thr} was completely modified by t⁶A37 in both cell types

(Fig. 5e and Supplementary Fig. 10c). As a control, we confirmed no reduction in t⁶A37 in mt-tRNA^{Ser}(AGY) and ct-tRNA^{Ile} isolated from patient fibroblasts (Supplementary Fig. 10d) and myoblasts (Supplementary Fig. 10e).

Taken together, these results are consistent with our in vitro mutation studies and demonstrate that pathogenic point mutations in mtDNA impaired t⁶A37 formation of mt-tRNA in patient cells, strongly indicating that the lack of t⁶A37 contributes to molecular pathogenesis of mitochondrial disease.

Because t⁶A37 is required for efficient m³C32 formation (Supplementary Fig. 5a), we measured the frequency of m³C32 in



mt-tRNA^{Thr} isolated from the patient's cells; the results revealed 44% in fibroblasts and 40% in myoblasts (Supplementary Fig. 5b). Thus, hypomodification at position 32 caused by loss of t⁶A37 might be an additional factor that contributes to mitochondrial disorders.

Mitochondrial t⁶A37 is sensitive to intracellular CO₂. We next measured the kinetic parameters for mitochondrial t⁶A37 formation on mt-tRNA^{Thr}, and determined apparent Km values for each substrate (Fig. 6a and Supplementary Table 2). The Km values for mt-tRNA^{Thr} were sub-micromolar (0.42 μM), indicating that OSGEPL1 has sufficient affinity for the tRNA substrate during t⁶A37 formation. By contrast, the Km values for ATP and L-Thr were 76 μM and 39 μM, respectively. Strikingly, the Km value (31 mM) for bicarbonate was quite high, but within the range of bicarbonate concentration (10–40 mM) in human mitochondria⁴⁹, indicating that mitochondrial t⁶A37 formation is sensitive to cellular bicarbonate concentration. Because bicarbonate is a substrate for TC-AMP formation catalyzed by YRDC³², we also measured the kinetic parameters for this reaction (Supplementary Table 3). The Km value for this reaction was 13 mM, demonstrating that mitochondrial TC-AMP formation also requires a high cellular concentration of bicarbonate.

For cell culture, we generally use DMEM medium, which contains 44 mM sodium bicarbonate, in a 5% CO₂ atmosphere, which should provide a sufficient concentration of bicarbonate in mitochondria. Indeed, under these conditions, high t⁶A frequency was observed in mt-tRNAs isolated from HEK293T cells (Figs. 2e and 3e, Supplementary Fig. 4). To determine whether the t⁶A37 frequency is regulated by bicarbonate concentration, we cultured HEK293T cells in medium without sodium bicarbonate in the absence of 5% CO₂ (air atmosphere) (Supplementary Fig. 11). Subsequently, four species of mt-tRNAs, along with ct-tRNA^{Ile}, were isolated and subjected to RNA-MS (Fig. 6b). The t⁶A37 frequency of mt-tRNA^{Ser(AGY)} decreased markedly from 58 ± 2.6% to 36 ± 3.5% ($P = 0.00018$) upon CO₂-depletion. We also found significant decrease of t⁶A frequency in mt-tRNA^{Asn} from 95 ± 1.8% to 81 ± 3.8% ($P = 0.00432$). Slight reduction of t⁶A was observed in mt-tRNA^{Lys} and mt-tRNA^{Thr} (Fig. 6b and Supplementary Fig. 12). However, no reduction of t⁶A was observed in ct-tRNA^{Ile} under CO₂-depleted conditions. The different responses of t⁶A37 formation in these mt-tRNAs to bicarbonate concentration might be due to differences in efficiency of t⁶A37 formation. As shown previously (Supplementary Fig. 8b), mt-tRNA^{Ser(AGY)} is a poorer substrate for OSGEPL1

than the other mt-tRNAs. Consistent with this, the rate of t⁶A37 formation of mt-tRNA^{Ser(AGY)} was much slower than that of mt-tRNA^{Thr} (Supplementary Fig. 13a). For mt-tRNA^{Ser(AGY)}, we monitored the t⁶A37 formation at increasing concentrations of bicarbonate (20–40 mM), revealing that the rate of t⁶A37 formation increased in response to the bicarbonate concentration (Supplementary Fig. 13b). Inefficient t⁶A37 formation in this mt-tRNA could be supported by higher concentrations of TC-AMP. This speculation provides a kinetic explanation for the observation that mt-tRNA^{Ser(AGY)} is sensitive to cellular bicarbonate concentration.

Rapidly growing tumors frequently fall into hypoxia due to low oxygen availability⁵⁰. Given that mitochondrial CO₂/bicarbonate is largely provided by TCA cycle, we asked whether mitochondrial t⁶A37 could be affected by hypoxic conditions in solid tumors. For these experiments, we prepared solid tumor xenografts by subdermally injecting colorectal adenocarcinoma HT-29 cells into nude mice, and then isolated and mt-tRNA^{Ser(AGY)} along with ct-tRNA^{Ile} for RNA-MS analyses. As shown in Supplementary Fig. 14, we detected hypomodification of t⁶A37 in mt-tRNA^{Ser(AGY)} isolated from the tumor, whereas high t⁶A frequency was observed in the same tRNA isolated from cell culture. This finding implies that t⁶A37 frequency can be modulated by hypoxic conditions in solid tumors.

Discussion

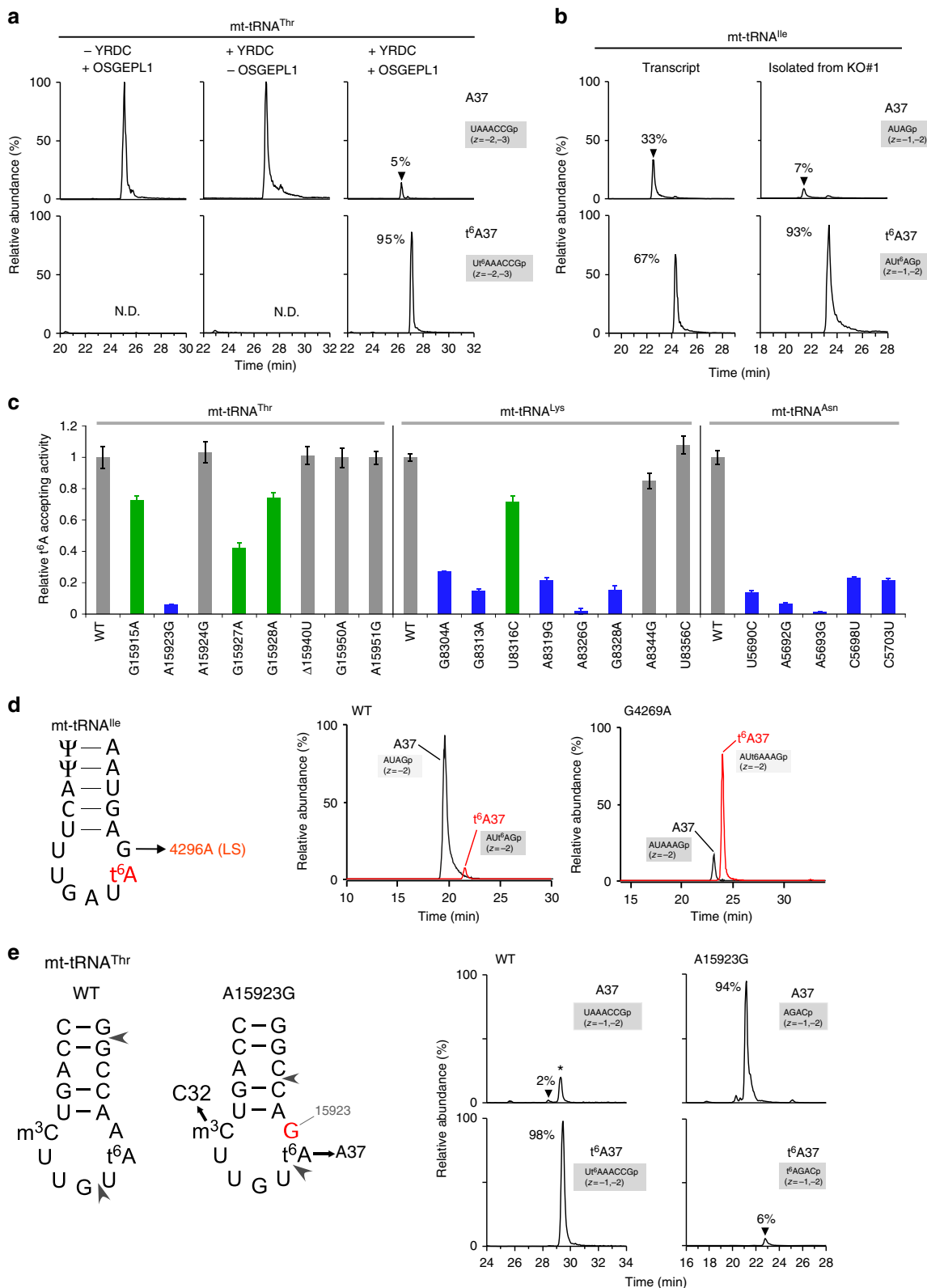
Here, we showed that YRDC and OSGEPL1 are required for t⁶A37 formation in mt-tRNAs. YRDC is predominantly localized in the cytoplasm, where it provides TC-AMP to the KEOPS complex to synthesize t⁶A37 in cytoplasmic tRNAs. However, YRDC contains a weak N-terminal MTS, and a certain fraction of YRDC is transported to mitochondria. In budding yeast, the YRDC homolog Sua5p is also localized in both cytoplasm and mitochondria⁵¹. A longer isoform of Sua5p translated from the upstream AUG codon has an MTS and enters mitochondria, while the smaller isoform translated from the downstream AUG codon at position 10 is predominantly localized in the cytoplasm. Although human YRDC also has the downstream AUG codon, it is not conserved among mammals (Supplementary Fig. 1a), indicating that the dual localization of YRDC in mammals and yeast operate via different mechanisms.

In OSGEPL1 KO strains, no t⁶A37 was formed in any of the five species of mt-tRNAs examined (Fig. 3e and Supplementary Fig. 4), although the steady-state levels of these mt-tRNAs were unchanged (Supplementary Fig. 7). The KO cells did not grow well in galactose medium (Fig. 4a), indicating minimal

Fig. 4 Mitochondrial dysfunction in OSGEPL1 KO cells. **a** Growth curves for WT HEK293T, OSGEPL1 KO#1, and OSGEPL1 KO#2 cells cultured in the presence of glucose (left) or galactose (right) as the primary carbon source. Mean values ± s.e.m. of four independent cultures are plotted. **b** Oxygen consumption rates of WT, OSGEPL1 KO#1, and OSGEPL1 KO#2 cells measured using an XFp extracellular flux analyzer. Mean values ± s.d. of biological triplicates are compared. * $P < 0.05$, Student's *t*-test. **c** Steady-state levels of ATP in WT, OSGEPL1 KO#1, and OSGEPL1 KO#2 cells. Mean values ± s.e.m. of three independent experiments are compared. * $P < 0.05$, Student's *t*-test. **d** Relative activities of respiratory complexes I, II, III, and IV (CI–IV) in WT, OSGEPL1 KO#1, and KO#2 cells. Mean values ± s.e.m. of three independent experiments are compared. * $P < 0.05$, Student's *t*-test. **e** Steady-state levels of subunit proteins in respiratory chain complexes. Mitochondrial fractions of WT, OSGEPL1 KO#1, and KO#2 cells resolved by SDS-PAGE were analyzed by western blotting with the indicated antibodies. A gel stained with Coomassie brilliant blue (CBB) is shown in Supplementary Fig. 6a. Uncut gel images are provided in Supplementary Fig. 15. **f** Pulse labeling of mitochondrial protein synthesis. WT, OSGEPL1 KO#1, and KO#2 cells were labeled with [³⁵S] methionine and [³⁵S] cysteine after cytoplasmic protein synthesis was halted with emetine. Whole-cell lysates were resolved by Tricine-SDS-PAGE and stained with CBB as a loading control (Supplementary Fig. 6b). The dried gel was exposed to an imaging plate and visualized on a fluorimager. Assignment of mitochondrial proteins is indicated. Uncut gel images are provided in Supplementary Fig. 15. **g** In vivo aminoacylation levels of mt-tRNA^{Lys} and mt-tRNA^{Val} in WT, OSGEPL1 KO#1, and OSGEPL1 KO#2 cells. Crude aminoacyl-tRNAs extracted under acidic conditions were treated with (+) or without (–) mild alkali for deacylation and subjected to acid urea-PAGE and northern blotting. White and black arrowheads indicate aminoacyl-tRNA and deacyl-tRNA, respectively. Aminoacylation level of each condition was calculated from the band intensities. Lysylation levels of mt-tRNAs^{Lys} from WT, KO#1, and KO#2 are 98.4%, 89.9%, and 83.9%, respectively. Valylation levels of mt-tRNAs^{Val} from WT, KO#1, and KO#2 are 90.1%, 90.3%, and 89.1%, respectively. Uncut gel images are provided in Supplementary Fig. 15

mitochondrial activity in these strains. Pulse-labeling experiments revealed that mitochondrial protein synthesis was markedly decreased by the absence of t⁶A37 (Fig. 4f). In particular, we observed severe reduction of protein synthesis for Complex I components, including ND1, ND2, ND4, ND5, and ND6 (Fig. 4f). In fact, steady-state levels of ND2 and ND5 decreased in

KO cells (Fig. 4e). Analysis of codon usage in 13 proteins encoded by mtDNA (Supplementary Table 4) revealed that the frequencies of the codons read by the five mt-tRNAs bearing t⁶A37 were higher in ND2 and ND5 than in the other genes. Thus, the lack of t⁶A37 reduces the decoding ability of the five mt-tRNAs, causing codon-specific dysfunction in mitochondrial translation. In



addition, the lysylation level of mt-tRNA^{Lys} was reduced in KO cells (Fig. 4g), indicating that t⁶A37 is required for efficient aminoacylation by lysyl-tRNA synthetase (KARS). Although the pleiotropic functions of t⁶A have been extensively studied in bacteria and yeast, this study provides the first evidence for a physiological role of t⁶A37 in human cells.

We successfully reconstituted t⁶A37 formation in vitro using recombinant YRDC and OSGEPL1. OSGEPL1 efficiently employed all five species of mt-tRNAs as substrates (Fig. 5a, b and Supplementary Fig. 8a, b), whereas *E. coli* enzymes only recognized three of the mt-tRNAs (Supplementary Fig. 8c). This observation indicates that OSGEPL1 has a broad substrate specificity that can accommodate the five mt-tRNAs with non-canonical clover leaf structures. However, in comparison with the other three substrates, mt-tRNA^{Ser(AGY)} and mt-tRNA^{Ile} were poor substrates for t⁶A37 formation (Fig. 5b and Supplementary Fig. 8b), indicating that OSGEPL1 is less able to recognize these two tRNAs. Because mt-tRNA^{Ile} lacking t⁶A37 isolated from OSGEPL1 KO cells was a better substrate for t⁶A37 formation than the in vitro transcribed mt-tRNA^{Ile} (Fig. 5b), it is likely that one or a combination of other modifications, m¹G9, m^{2,2}G26, Ψ27, and Ψ28, in mt-tRNA^{Ile} (Fig. 1b) supports efficient t⁶A37 formation mediated by OSGEPL1. The observation that each mt-tRNA exhibited a different t⁶A37 formation activity implies that mitochondrial translation is regulated in a codon-specific manner.

Pathogenic mutations in mt-tRNAs associated with mitochondrial diseases frequently impair post-transcriptional modifications in mt-tRNAs, resulting in dysfunction of mitochondrial protein synthesis. We previously reported the absence of tm⁵U34 in mt-tRNA^{Leu(UUR)} with each of five pathogenic point mutations associated with MELAS, and the absence of tm⁵s²U34 in mt-tRNA^{Lys} with one pathogenic mutation associated with MERRF⁷. In addition, we found two pathogenic point mutations that impair t⁶C34 formation in mt-tRNA^{Met5252}. In this study, we examined the impact of 22 pathogenic point mutations in three mt-tRNAs on t⁶A37 formation in vitro and found 15 mutations that impaired or reduced t⁶A37 formation (Fig. 5c). As expected, we detected little t⁶A37 formation in mt-tRNA^{Lys} bearing the A8326G mutation or in mt-tRNA^{Asn} bearing the A5693G mutation because these two variants are target site mutations at position 37 (Fig. 1b). Similarly, no t⁶A37 would be expected in mt-tRNA^{Ile} bearing the target site mutation (A4295G). Many mutations that impaired t⁶A37 formation reside in the anticodon stem-loop of mt-tRNAs. In mt-tRNA^{Lys}, mutations in the D-stem also affected t⁶A37 formation, indicating that OSGEPL1 recognizes the sequence and/or structure of the anticodon stem-loop and D-stem in mt-tRNAs. In particular, A15923G in mt-tRNA^{Thr}

and A5692G in mt-tRNA^{Asn} strongly impaired t⁶A37 formation. Because both mutations are located at position 38, A38 (which is 3' adjacent to the target site) (Fig. 1b) acts as a positive determinant for t⁶A37 formation. Indeed, we found little t⁶A37 in mt-tRNA^{Thr} with the A15923G mutation isolated from the patient's cells with MERRF-like symptoms (Fig. 5e and Supplementary Fig. 10c). These results demonstrate that pathogenic point mutations in mt-tRNAs inhibit t⁶A37 formation, leading to deficient decoding activity and tRNA function in mitochondrial protein synthesis.

Intriguingly, mt-tRNA^{Ile} naturally contains G38 (G4296) (Fig. 1b) which should work as a negative determinant for t⁶A37 formation, as observed in A-to-G pathogenic point mutations at the corresponding positions in mt-tRNA^{Thr} and mt-tRNA^{Asn}. This feature nicely explains why mt-tRNA^{Ile} is a poor substrate for OSGEPL1. G4296A has been reported as a pathogenic mutation associated with Leigh syndrome, juvenile Parkinsonism, and hypogonadism^{48, 53, 54}. Here, we revealed that this pathogenic mutation markedly improved t⁶A37 formation of mt-tRNA^{Ile} in vitro (Fig. 5d), suggesting that G38 has an attenuator function that regulates t⁶A37 frequency. Under normal culture conditions, mt-tRNA^{Ile} has a higher frequency (over 90%) of t⁶A37 (Fig. 2e and Supplementary Fig. 4), indicating that other modifications might contribute to efficient recognition by OSGEPL1 (Fig. 5b). Among 282 mtDNAs in mammalian species reported so far, A37 and G38 in mt-tRNA^{Ile} are conserved in 280 species⁵⁵, suggesting that the regulatory effect of G38 on t⁶A37 formation plays a physiological role in certain biological contexts and conditions.

Kinetic studies of t⁶A37 formation revealed that the Km value of bicarbonate (31 mM) was extremely high (Fig. 6a and Supplementary Table 2), whereas the Km values of other substrates required for t⁶A37 formation were in the micromolar range. For TC-AMP formation catalyzed by YrdC, L-Thr needs to form a carbamate (*N*-carboxy-L-Thr), followed by adenylation³². It is known that amino acids form carbamates at high concentration of bicarbonate or CO₂ at alkaline pH non-enzymatically⁵⁶. The high Km value of bicarbonate for TC-AMP and t⁶A37 formation can be explained by the carbamate formation of L-Thr at the initial step of the reaction. Considering that mitochondrial bicarbonate concentration ranges from 10 to 40 mM⁴⁹ ([S]/Km for bicarbonate = 0.32–1.3), the frequency of t⁶A37 in mt-tRNAs should be regulated by intracellular bicarbonate concentrations. When HEK293T cells were cultured with non-bicarbonate medium in an air atmosphere, the levels of t⁶A37 in mt-tRNAs were reduced (Fig. 6b). Because ct-tRNA^{Ile} retained a high frequency of t⁶A37 under this culture condition, bicarbonate-sensitive t⁶A37 formation is specific for mt-tRNAs. Although most of the

Fig. 5 In vitro reconstitution of t⁶A37 on mt-tRNAs and impairment of t⁶A37 by pathogenic point mutations associated with mitochondrial diseases. **a** In vitro formation of t⁶A37 on mt-tRNA^{Thr} transcripts with or without YRDC and OSGEPL1 in the presence of Thr, ATP, and bicarbonate. After the reaction, mt-tRNA^{Thr} was digested with RNase T₁ and analyzed by LC/MS. XICs generated by integration of multiply-charged negative ions of A37-containing fragments of mt-tRNA^{Thr} harboring A37 (top) and t⁶A37 (bottom) (Supplementary Table 1). Intensity fractions (%) of modified or unmodified fragments are denoted. N.D., not detected. **b** In vitro formation of t⁶A37 on mt-tRNA^{Ile} transcript or native mt-tRNA^{Ile} isolated from OSGEPL1 KO#1 cells. XICs generated by integration of multiply-charged negative ions of A37-containing fragments of mt-tRNA^{Ile} harboring A37 (top) and t⁶A37 (bottom) (Supplementary Table 1). Intensity fractions (%) of modified or unmodified fragments are denoted. **c** Efficiency of t⁶A37 formation in mt-tRNA mutants. The numbering of each mutant corresponds to that in Fig. 1b. Bars corresponding to severe and mild reduction in t⁶A37 formation are colored in blue and green, respectively. **d** G4296A in mt-tRNA^{Ile} (left panel) is a unique pathogenic mutation that promotes t⁶A37 formation. XICs show A37-containing fragments of WT and G4296A mutant mt-tRNA^{Ile} harboring A37 (black) and t⁶A37 (red). *m/z* values of each fragment are listed in Supplementary Table 1. **e** Impairment of t⁶A37 in mt-tRNA^{Thr} with A15923G mutation isolated from the myoblasts of a patient with MERRF-like symptoms. Anticodon stem-loop sequences of WT (left) and A15923G mutant (right) mt-tRNA^{Thr}. Positions of RNase T₁ and RNase A digestion are indicated by arrowheads. m³C32 in the A15923G mutant is partially converted to C32 (Supplementary Fig. 5b). XICs generated by integration of multiply-charged negative ions of A37-containing fragments of mt-tRNA^{Thr} harboring A37 (upper panels) and t⁶A37 (lower panels) (Supplementary Table 1) from WT (left panels) and A15923G myoblasts (right panels). Intensity fractions (%) of modified or unmodified fragments are indicated

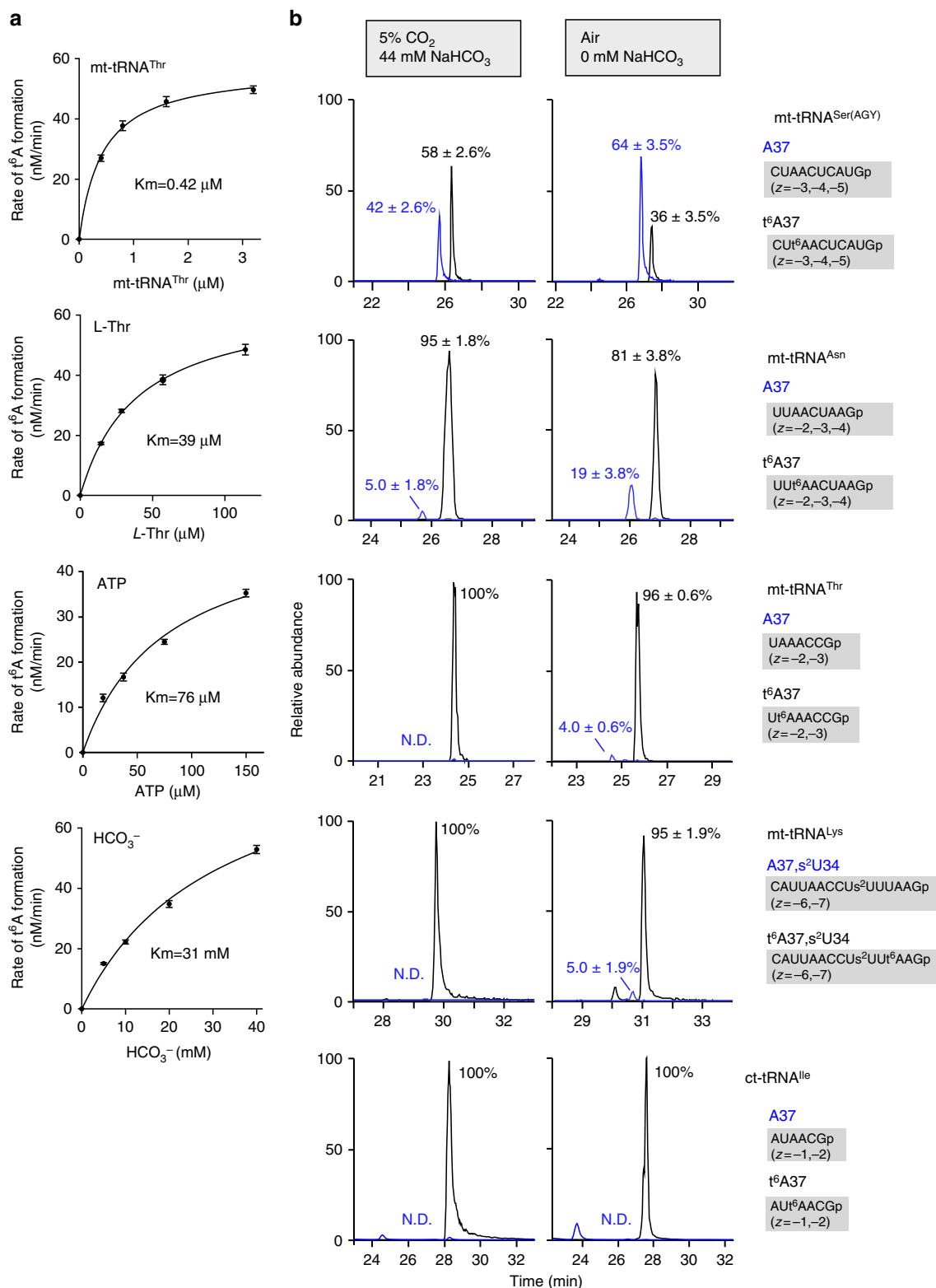


Fig. 6 Mitochondrial t⁶A37 formation is sensitive to intracellular bicarbonate concentration. **a** Kinetic analyses of mitochondrial t⁶A37 formation mediated by YRDC and OSGEPL1. Initial velocities of t⁶A37 formation were measured against variable concentrations of mt-tRNA^{Thr}, L-Thr, ATP, and bicarbonate. Km values for each substrate are indicated. **b** Hypomodification of t⁶A37 in mt-tRNAs in HEK293T cells cultured in non-bicarbonate medium. XICs generated by integration of multiply-charged negative ions of A37-containing fragments of mt-tRNA^{Ser(AGY)} (top panels), mt-tRNA^{Asn} (second panels), mt-tRNA^{Thr} (third panels), mt-tRNA^{Lys} with s²U34 (fourth panels) and ct-tRNA^{Ile} (bottom panels) bearing A37 (blue) and t⁶A37 (black) (Supplementary Table 1) isolated from HEK293T cells cultured with normal DMEM medium (44 mM NaHCO₃) in 5% CO₂ (left panels) and non-bicarbonate medium in air (right panels). mt-tRNA^{Ser(AGY)} and other tRNAs were isolated from the cells cultured for 6 and 3 days, respectively. t⁶A frequencies (%) are described as mean values ± s.d. of technical triplicate

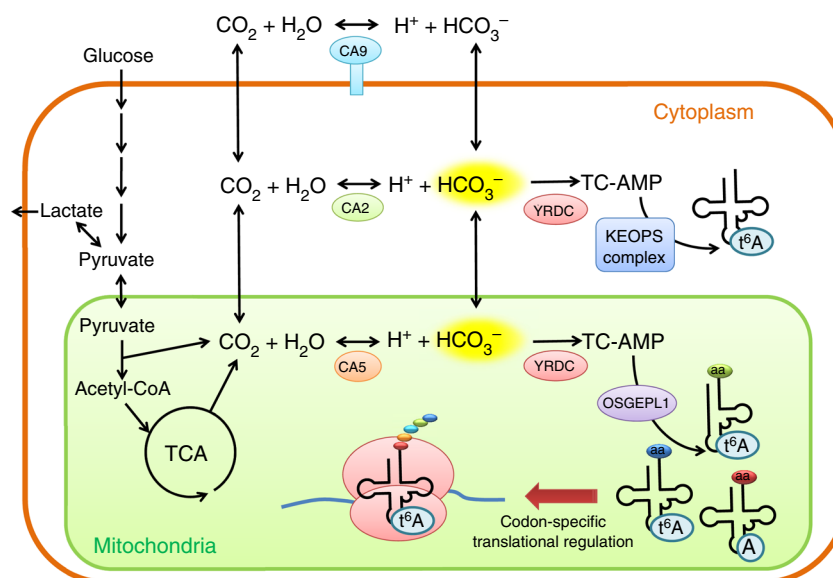


Fig. 7 Metabolism of bicarbonate and t⁶A37 formation in cytoplasm and mitochondria. CO₂ produced by TCA cycle is hydrated to form bicarbonate by carbonic anhydrase 5 (CA5) in mitochondria. In addition, mitochondrial CO₂ is exported to cytoplasm and hydrated by carbonic anhydrase 2 (CA2). In hypoxic conditions, carbonic anhydrase 9 (CA9) is overexpressed on the cell surface by HIF-1 pathway. CA9 generates large amounts of bicarbonate outside the cell. Then, cells actively import extracellular bicarbonate to neutralize lactate and prevent acidification. YRDC employs bicarbonate to synthesize TC-AMP, which is used for t⁶A37 formation on tRNAs mediated by KEOPS complex in cytoplasm and by OSGEPL1 in mitochondria. Hypomodification of t⁶A37 in two mt-tRNAs in the cells cultured without bicarbonate, as well as from hypoxic solid tumors, indicating codon-specific translational regulation by sensing intracellular bicarbonate

mitochondrial bicarbonate is assumed to originate from CO₂ produced by respiration in the mitochondria, extracellular bicarbonate supplied in the medium is required to maintain high t⁶A37 frequency in mt-tRNAs. HeLa cells require a sufficient concentration of bicarbonate in the medium to engage in rapid proliferation⁵⁷, indicating that respiratory CO₂ in mitochondria is not sufficient to support cell growth. Considering that t⁶A37 has pleiotropic functions in protein synthesis, we presume that bicarbonate-sensitive t⁶A37 formation contributes to codon-specific translational regulation in mitochondria via sensing of respiratory activity and extracellular bicarbonate concentration. In particular, when mitochondrial respiration decreases, intake of extracellular CO₂ or bicarbonate is necessary to support cell viability (Fig. 7). Rapidly proliferating solid tumors frequently outgrow their blood supply, leading to a hypoxic microenvironment in the inner region of the tumor due to low oxygen availability⁵⁸. In this situation, the mitochondrial concentration of bicarbonate should be reduced because TCA cycle is inhibited⁵⁹. In fact, we observed hypomodified t⁶A37 in mt-tRNA^{Ser(AGY)} isolated from HT-29 xenografts (Supplementary Fig. 14), implying that mitochondrial bicarbonate is not sufficient to support efficient t⁶A37 formation in mt-tRNAs in hypoxic tumors. Under hypoxic conditions, HIF-1 α is stabilized and activates a set of genes related to anaerobic glycolysis⁶⁰, resulting in massive accumulation of lactate in the cell. In addition, carbonic anhydrase 9 (CA9) is overexpressed on the cell surface as a consequence of HIF-1 α stabilization, and plays a critical role in generating large amounts of bicarbonate and protons (Fig. 7)⁶¹. Cells actively take up extracellular bicarbonate to neutralize lactate and prevent acidification; in addition, bicarbonate is used to support high frequency of t⁶A37 in cytoplasmic tRNAs (Fig. 6b and Supplementary Fig. 14). At the same time, mitochondria are thought to import bicarbonate from cytoplasm to maintain levels of t⁶A37 in mt-tRNAs (Fig. 7). However, we clearly detected hypomodification of t⁶A37 in mt-tRNAs (Fig. 6b and Supplementary Fig. 14), indicating that mitochondrial t⁶A37 formation

serves as a sensor function to monitor hypocarbia conditions. Given that hypomodification of t⁶A37 in mt-tRNAs down-regulates mitochondrial translation at codon-specific manner, CO₂ sensitivity of t⁶A37 might be a part of Warburg effect⁶² to control oxidative phosphorylation (OXPHOS) activity via translational regulation in mitochondria under hypoxic condition.

In this study, we showed that YRDC and OSGEPL1 are required for t⁶A37 formation in five mt-tRNAs and that t⁶A37 plays critical roles in protein synthesis and respiratory activities in mitochondria. Kinetic studies revealed that mitochondrial t⁶A37 formation is dynamically regulated by cellular bicarbonate concentration. In support of this finding, we observed hypomodification of t⁶A37 in mt-tRNA isolated from human cells cultured with non-bicarbonate medium, as well as hypoxic solid tumors, implying codon-specific regulatory translation under hypoxic conditions. We also identified pathogenic point mutations that impaired t⁶A37 formation in mt-tRNAs and confirmed low levels of t⁶A37 in mt-tRNA^{Thr} with the A15923G mutation isolated from a patient with MERRF-like symptoms, indicating that the lack of t⁶A37 has pathological consequences.

Methods

Cell culture and growth measurement. HEK293T, HeLa, HT-29, fibroblast, and myoblast cells were cultured at 37 °C in 5% CO₂ in DMEM (D5796, Sigma) supplemented with 10% or 20% FBS (Gibco). The viable cell numbers were counted by trypan blue staining assay.

Growth of HEK293T cells was measured using AlamarBlue (Invitrogen) in glucose medium (Wako DMEM 042-32255 supplemented with 10% FBS and 1 mg/mL glucose) or galactose medium (Wako DMEM 042-32255 supplemented with 10% FBS and 1 mg/mL galactose). Cells were inoculated at a density of 2.0×10^3 cells/well on collagen I-coated 96-well plates (Iwaki). On each day of cell cultivation (days 0 to 6), 1/10 volume of AlamarBlue reagent was added to each well and incubated for 4 h; absorbance was then measured at 570 nm and 600 nm using a SpectraMax 190 microplate reader (Molecular Devices).

For growth measurement in non-bicarbonate medium, bicarbonate-free DMEM (D5648, Sigma) was supplemented with 10% FBS (Gibco), 30 mM HEPES (Rikaken), and 10 μ g/mL each of nucleosides (adenosine, cytidine, guanosine, and uridine), and adjusted to pH 7.1 with NaOH. To add back bicarbonate, the non-bicarbonate medium was supplemented with 44 mM NaHCO₃, and adjusted to pH

7.2 with HCl. HEK293T cells precultured in DMEM were suspended in the non-bicarbonate medium. Cells were seeded at a density of 4×10^5 cells/well on 96-well cell culture plates (TrueLine), and cultured at 37 °C under air (~0.04% CO₂) for the non-bicarbonate medium, and under 5% CO₂ for the bicarbonate-added back medium, respectively. On each day of cell culture, 1/10 volume of 1.4 mM resazurin sodium salt (Nacalai Tesque) dissolved in PBS was added to each well and incubated for 3 h. Fluorescence was then measured with excitation/emission at 550/600 nm using an Infinite 200 Pro M Plex (TECAN).

To estimate CO₂ effect on t⁶A frequency, HEK293T cells were cultured in the non-bicarbonate medium with or without 44 mM NaHCO₃ as described above, under 5% CO₂ or air (~0.04% CO₂), respectively, at 37 °C for 3 days. For mt-tRNA^{Ser(AGY)}, prolonged cultivation was conducted as following. The cells were seeded in 15 cm dishes and pre-cultured to 70% confluence at 37 °C in 5% CO₂ in DMEM (D5796, Sigma) supplemented with 10% FBS (Gibco). Then, the cells were washed twice with non-bicarbonate medium consisted of bicarbonate-free DMEM (D5648, Sigma), 10% FBS (Gibco), 30 mM HEPES-NaOH (pH 7.4), and 10 µg/mL each of nucleotides (adenosine, cytidine, guanosine, and uridine) (final, pH 7.2), and then cultured with the same medium at 37 °C without CO₂ (air atmosphere) for 6 days. The medium was exchanged every 3 days. Total RNA was extracted, individual tRNAs were isolated, and tRNA modifications were analyzed by MS as described below.

Construction of knockout cell lines. *OSGEPL1* KO cells were generated using the CRISPR/Cas9 system as described previously^{52, 63}. Sense and antisense oligonucleotides for a guide RNA (sgRNA) (Supplementary Data 1) were cloned into vector pX330 (Addgene plasmid 42230)⁶⁴. HEK293T cells were transfected with a pX330 vector bearing the sgRNA sequence and with pEGFP-N1 (Clontech) and pLL3.7 vectors containing the puromycin resistance gene; transfections were performed using FuGENE HD (Promega). One day after transfection, cells were seeded at low density, and transfectants selected with 1 µg/mL puromycin. Knockout lines were selected by the surveyor assay. The target region of the genome in each clone was PCR-amplified using primers listed in Supplementary Data 1 and sequenced.

RNA extraction and isolation of individual tRNAs. Total RNA from culture cells was extracted using TriPure Isolation Reagent (Roche). For acid-urea PAGE-northern blotting⁶⁵ to detect aminoacylation levels of tRNAs, total RNA was obtained by phenol extraction under acidic conditions using 50 mM NaOAc (pH 5.3) at 4 °C.

Individual tRNAs were isolated by reciprocal circulating chromatography as described^{22, 44} using the DNA probes listed in Supplementary Data 1.

Mass spectrometry. Liquid chromatography-mass spectrometry (LC/MS) analyses of tRNA fragments were performed as described previously^{22, 45}. Around 1 pmol of each isolated tRNA was digested at 37 °C for 30 min with 50 units RNase T₁ (Thermo Scientific) in 20 mM NH₄OAc (pH 5.3) or 10 ng RNase A (Ambion) in 20 mM NH₄OAc (pH 7.7), followed by addition of an equal volume of 0.1 M triethylamine acetate (TEAA; pH 7.0). The digest (800 fmol) was subjected to the trap column for desalting and chromatographed by a HiQ sil C18W-3 nano spray column (C18, 3 µm, 120 Å pore size; ID 0.1 × 100 mm, KYA Technologies) with solvent system consisted of 0.4 M 1,1,1,3,3,3-hexafluoro-2-propanol (HFIP) (pH 7.0) (solvent A) and 0.4 M HFIP (pH 7.0) in 50% methanol (solvent B) at a flow rate of 300 nL/min with a linear gradient of 5–100% B over 35 min with a splitless nano HPLC system (DiNa, KYA Technologies). The eluent was ionized by ESI source, and directly introduced into an iontrap-orbitrap hybrid mass spectrometer (LTQ Orbitrap XL, Thermo Fisher Scientific). Ions were scanned with a negative polarity mode over an *m/z* range of 600–2000 throughout the separation. Exact molecular mass and its multiply-charged negative ions of the t⁶A37-containing RNA fragment in each tRNA was calculated by accurate atomic composition. Modification frequency was calculated by peak area ratio of mass chromatograms of modified versus unmodified fragments.

For estimation of ESI detection efficiencies of RNA fragments with and without t⁶A modification, human mt-tRNA^{Leu} isolated from WT HEK293T cells and its unmodified one isolated from *OSGEPL1* KO cells (KO#2) were mixed with different ratio (total quantity is adjusted to 1 pmol in each sample), digested by RNase T₁ and subjected to LC/MS. The peak area ratio of the A37-containing fragments with and without t⁶A was plotted against the mixing ratio for each sample (Supplementary Fig. 3). Then, t⁶A frequency of the native mt-tRNA^{Leu} was calculated with the slope of this plot, and the mixing ratios were transformed to t⁶A frequencies. The resulting plot of t⁶A frequency versus intensity ratio is depicted in Supplementary Fig. 3.

YRDC or *OSGEPL1*, immunoprecipitated with an anti-FLAG-tag antibody, was resolved by SDS-PAGE. Cys residues were alkylated by iodoacetic acid, followed by digestion with sequencing grade trypsin or AspN (Promega) using an in-gel digestion method. The digested peptides were then subjected to capillary LC/nano ESI-MS as previously described⁶⁶.

Expression and purification of recombinant proteins. For protein expression in HeLa or HEK293T cells, cDNAs of YRDC (NM_024640.3) and *OSGEPL1*

(NM_022353.2) were amplified by RT-PCR with sets of primers (Supplementary Data 1) and cloned into vector pDEST12.2 with a C-terminal FLAG-tag using the pENTR/D-topo Gateway cloning kit (Invitrogen). Transfection of plasmids was conducted using FuGENE HD reagent (Promega) or linear polyethylenimine.

For construction of recombinant proteins, three isoforms of YRDC (full length, 17–279a.a. and 52–279a.a.) were cloned into vector pE-SUMO using the indicated primers (Supplementary Data 1). The recombinant YRDC fused with N-terminal His6-SUMO was overexpressed in the *E. coli* Rosetta (DE3) strain (Novagen) cultured in LB medium and induced with 10 µM IPTG at 22 °C overnight. The N-terminal His6-SUMO tagged YRDC was purified from the cell lysate using a HisTrap HP column (GE Healthcare) on an AKTA purifier 10 system (GE Healthcare). Recombinant protein was digested with TEV protease (Promega) and applied on the HisTrap column to remove the His₆-SUMO tag. The flow-through fraction was dialyzed in buffer containing 50 mM HEPES-KOH (pH 7.5), 100 mM KCl, 2 mM MgCl₂, and 1 mM DTT, followed by addition of glycerol (final concentration, 20%) and storage at –30 °C.

OSGEPL1 (35–414a.a.) was cloned into pET28a (Novagen) using a set of primers (Supplementary Data 1). The C-terminal His6-tagged *OSGEPL1* was overexpressed in the *E. coli* Rosetta (DE3) strain (Novagen) cultured in LB medium and induced with 100 µM IPTG at 28 °C overnight. Soluble *OSGEPL1* was trapped on a HisTrap HP column (GE Healthcare), further purified on a MonoQ column (GE healthcare), and stored as described above.

Western blotting and antibodies. Mitochondrial fractions were isolated from WT and *OSGEPL1* KO HEK293T cells (1×10^7 cells) using the Mitochondria Isolation Kit (Miltenyi Biotec, K.K.) and subjected to western blotting to measure steady-state levels of protein components in respiratory chain complexes using the Total OXPHOS Rodent WB Antibody Cocktail (an antibody mixture targeting ATP5A, UQCRC2, MTCO1, SDHB, and NDUFB8; ab110413, Abcam), an anti-ND5 antibody (ab92624, Abcam), and an anti-ND2 antibody (19704-1-AP, Proteintech). Other antibodies used in this study were as follows: anti-*OSGEPL1* (25694-1-AP, Proteintech), anti-GAPDH (6C5, Santa Cruz Biotech), anti-FLAG-tag (1E6, Wako), HRP-conjugated donkey anti-mouse/rabbit IgG (715-035-150/715-035-152, Jackson ImmunoResearch), anti-FLAG M2 affinity gel (A2220, Sigma), and Alexa Fluor 488-conjugated goat anti-mouse IgG (A-11001, ThermoFisher). To monitor YRDC subcellular localization using the anti-FLAG-tag antibody, mitochondrial fractions were carefully washed with 2 mg/mL digitonin (Sigma) to remove the outer membrane with cytoplasmic components.

Northern blotting. Total RNA (2 µg) from cultured cells was dissolved by 10% denaturing PAGE, stained with SYBR Gold (Invitrogen), and blotted onto a nylon membrane (Amersham Hybond N+; GE Healthcare) in 1× TBE using a Transblot Turbo apparatus (Bio-Rad). The membrane was air-dried and irradiated twice with UV light (254 nm, 120 mJ/cm²; CL-1000, UVP) to crosslink the blotted RNA. Hybridization was performed essentially according to the manufacturer's instructions (PerfectHyb, TOYOBO) at 52 °C with 4 pmol of 5'-³²P-labeled oligonucleotides (Supplementary Data 1) specific for each mt-tRNA. The membrane was washed three times with 1× SSC, dried, and exposed to an imaging plate (BAS-MS2040, Fujifilm). Radioactivity was visualized using an FLA-7000 imaging analyzer (Fujifilm).

Preparation of mt-tRNA transcripts. A series of tRNA mutants were synthesized by in vitro transcription using T7 RNA polymerase⁶⁷. DNA templates for in vitro transcription were constructed by PCR using a series of oligo DNAs (listed in Supplementary Data 1). All mt-tRNA transcripts were gel-purified.

In vitro reconstitution of t⁶A37. In vitro reconstitution of t⁶A37 on tRNA was carried out at 37 °C for 1 h in a 20-µL reaction mixture containing 100 mM Tricine-NaOH (pH 8.0), 2 mM DTT, 15 mM MgCl₂, 1 mM ATP, 5 mM L-Thr, 40 mM NaHCO₃, 1 µM mt-tRNA, 1 µM YRDC (17–279a.a.), and 2 µM *OSGEPL1* (35–414a.a.). The mt-tRNAs were extracted with phenol/chloroform/isoamyl alcohol (25:24:1, pH 5.2) (Nacalai Tesque), dialyzed, digested with RNase T₁, and subjected to LC/MS analyses to detect and quantify t⁶A37 formation.

For kinetic analyses, initial velocity of t⁶A37 formation was measured at 37 °C in a 10-µL reaction mixture (for each data point) containing 100 mM Tricine-NaOH (pH 8.0), 2 mM DTT, 15 mM MgCl₂, 18.75–150 µM ATP, 14.275–114.2 µM [¹⁴C] L-Thr, 5–40 mM NaHCO₃, 0.4–3.2 µM mt-tRNA, 1 µM YRDC (17–279a.a.), and 2 µM *OSGEPL1* (35–414a.a.). To stop the reaction, the mixture was spotted on a Whatman 3MM filter paper, soaked in 5% TCA, washed three times with 5% TCA, and rinsed with ice-cold ethanol. Radioactivity of [¹⁴C] L-Thr on the dried paper was measured by liquid scintillation counting on a Tri-Carb 2810TR (PerkinElmer).

Kinetic analysis of TC-AMP formation. TC-AMP is an unstable compound with a short half-life³². To measure kinetic parameters of TC-AMP formation catalyzed by YRDC, we converted TC-AMP to N-carboxythreonyl anhydride (Thr-NCA) under mild alkaline conditions (pH 8.2). Thr-NCA is stable enough to be detected and quantified by thin layer chromatography (TLC). Thr-NCA formation was

carried out at 37 °C in a 10- μ L reaction mixture (for each data point) containing 50 mM Tricine-NaOH (pH 8.5), 10 mM MgCl₂, 1 mM ATP, 100 mM NaHCO₃, and 2 mM [¹⁴C] L-Thr. For kinetic analyses, the concentration of each substrate was altered to 0.1–0.8 mM ATP, 10–80 mM NaHCO₃, and 50–400 μ M L-Thr, respectively. To stop the reaction, 0.1 volume of acetic acid was mixed with the solution for each period of time. Aliquots were spotted on silica gel TLC plate (Merck) which was then developed by a solvent consisted of *n*-butanol:acetic acid:water = 4:1:1. Radioactivity of [¹⁴C] Thr-NCA on the TLC plate was visualized using an imaging plate (BAS-MS2040, Fujifilm) on a fluorimager (FLA-7000, Fujifilm).

Mitochondrial activities. For mitochondrial isolation, WT or *OSGEPL1* KO HEK293T cells (5×10^7) were homogenized in 3 mL of low buffer (80 mM sucrose, MOPS-NaOH (pH 7.2)) and mixed with equal volume of high buffer (250 mM sucrose, 10 mM MOPS-NaOH (pH 7.2)), followed by centrifugation at 600 *g* for 15 min. The supernatant was collected, homogenized again, and centrifuged at 10,000 \times *g* for 20 min to collect the mitochondrial fraction as a pellet. The resultant mitochondrial fraction was used to measure complex activities as described⁶⁸. For Complex I, a reaction mixture (1 mL) consisting of 40 μ g/mL mitochondria, 50 mM KH₂PO₄-KOH (pH 7.4), 1 mM KCN, 50 μ M CoQ1, and 75 μ M NADH was incubated at 32 °C, and absorbance at 340 nm was monitored by UV-visible spectrophotometer V-630 equipped with a temperature control unit PAC-743R (JASCO). As a negative control, the reaction mixture containing 20 μ M rotenone was used. For Complex II, a reaction mixture (1 mL) consisting of 40 μ g/mL mitochondria, 50 mM KH₂PO₄-KOH (pH 7.4), 20 mM succinate (pH7.2), 5 μ g/mL antimycin, 50 μ M rotenone, 2 mM KCN, 50 μ M 2,6-dichloro-ophenolindophenol (DCPIP), and 50 μ M decylubiquinone (DB) was incubated at 32 °C, and absorbance at 600 nm was monitored. For measurement of Complex III, reduced DB was prepared as follows: 50 μ L of 10 mM DB, 5 μ L of 0.1 M HCl, and a small piece of potassium borohydride were mixed and incubated at room temperature. Followed by centrifugation, the supernatant was mixed with 5 μ L of 1 M HCl. Complex III activity was monitored by absorbance at 550 nm at 32 °C in 1 mL reaction mixture consisting of 40 μ g/mL mitochondria, 6 μ L of reduced DB, 50 μ M cytochrome C (CytoC), 10 mM KH₂PO₄-KOH (pH 7.4), 2 mM EDTA, 4 μ M rotenone, and 2 mM KCN. For measurement of Complex IV, reduced CytC was prepared as follows: 1 mL of 2.7 mg/mL CytoC and 50 μ L of 0.1 M DTT were mixed and reacted at room temperature for 15 min. Complex IV activity was monitored by absorbance at 550 nm at 32 °C in 1 mL reaction mixture consisting of 40 μ g/mL mitochondria, 10 mM KH₂PO₄-KOH (pH 7.4), and 129 μ g/mL reduced CytoC.

To measure the ATP levels, WT or *OSGEPL1* KO HEK293T cells were seeded in 96-well optical-bottom plates (10⁴ cells/well). After 20 h incubation at 37 °C in 5% CO₂, total ATP in each well was measured using luciferin-luciferase assay solution (CA100, TOYO INK) to calculate the relative ATP levels. Luminescence was detected using a GLOMAX96 Microplate Luminometer (Promega).

Oxygen consumption rates (OCRs) of WT or *OSGEPL1* KO HEK293T cells were measured using an XFp extracellular flux analyzer (Seahorse Bioscience) as described previously³². WT and *OSGEPL1* KO cells were seeded in 3 wells each (3×10^5 cells/well) of an XF24 cell culture miniplate, which is manually coated with collagen, and cultured for 24 h and changed the medium (25 mM glucose, 1.25 mM pyruvic acid, pH 7.4 by NaOH). OCR of each well was measured without any inhibitors.

Pulse labeling of mitochondrial translation. The pulse labeling of mitochondrial protein synthesis was performed essentially as described⁶⁹. WT or *OSGEPL1* KO HEK293T cells (2×10^6 cells) were cultured at 37 °C for 15 min in 6 mL of L-glutamine/L-cysteine-free DMEM (21013-024, Gibco) containing 10% dialyzed FBS (Gibco), 2 mM L-glutamine (Sigma), and 1 mM sodium pyruvate (Gibco), followed by addition of 77 μ g/mL emetine (Sigma) and incubation for 5 min. Then, Easy Tag Express Protein Labeling Mix [³⁵S] (NEG772007MC, Perkin Elmer) was added and the sample incubated at 37 °C for 1 h to specifically label mitochondrial proteins. Cell lysates (100 μ g total proteins) were resolved by Tricine-SDS-PAGE (16.5%) and the gel was CBB-stained and dried on a gel drier (AE-3750 RapiDry, ATTO). Radiolabeled mitochondrial protein products were visualized by exposure to an imaging plate (BAS-MS2040, Fujifilm) on a fluorimager (FLA-7000, Fujifilm).

Tumor xenograft. HT-29 cells (5×10^6 cells) were transplanted subdermally into BALB/c nude mice (female, 6 week old). Three weeks after the transplantation, the tumors were removed and subjected to RNA extraction. All the animal protocols were approved by the safety division of RIKEN.

Case report and clinical course for the A15923G mutation. The patient was a female and aged 15 years and 1 month at the time of sample collection. At age 6, she was diagnosed with bilateral hearing impairment, which became progressively worse from around the age of 8 years. She started to use hearing aids at age 9 and underwent cochlear implant surgery at the age of 10 years and 11 months. At around age 10, short stature was noted and a detailed examination was conducted. MRI and CT scans of the head revealed calcification of the bilateral dentate nuclei, caudate nuclei, putamina, globi pallidi, and thalami. She also had elevated levels of

lactic acid/pyruvic acid in the blood (23.6/0.87 mg/dL) and spinal fluid (35.0/1.29 mg/dL), pigmentary degeneration of the retina, and proteinuria; consequently, mitochondrial disease was suspected. At around age 12, the patient started to have myoclonic seizures and generalized seizures triggered by visual stimuli such as light. The electroencephalogram (EEG) revealed spike-and-wave discharges (approximately 3 Hz), and treatment with anti-seizure medication was initiated. The clinical course and symptoms were suggestive of MERRF. Occasional headaches were also observed. At the age of 12 years and 10 months, she underwent a muscle biopsy and the muscle pathology revealed scattered cytochrome-*c*-oxidase-negative ragged-red fibers. Full mitochondrial DNA sequencing detected essentially homoplasmic m.15923A >G mutation in muscle. Based on these findings, the diagnosis of mitochondrial disease was established. This study was approved by the IRB of National Center of Neurology and Psychiatry.

Data availability. The data supporting the findings in this study are available from the corresponding author upon reasonable request.

Received: 13 April 2017 Accepted: 16 April 2018

Published online: 14 May 2018

References

- Chen, K., Zhao, B. S. & He, C. Nucleic acid modifications in regulation of gene expression. *Cell Chem. Biol.* **23**, 74–85 (2016).
- Frye, M., Jaffrey, S. R., Pan, T., Rechavi, G. & Suzuki, T. RNA modifications: what have we learned and where are we headed? *Nat. Rev. Genet.* **17**, 365–372 (2016).
- Machnicka, M. A. et al. MODOMICS: a database of RNA modification pathways--2013 update. *Nucleic Acids Res.* **41**, D262–D267 (2013).
- El Yacoubi, B., Bailly, M. & de Crécy-Lagard, V. Biosynthesis and function of posttranscriptional modifications of transfer RNAs. *Annu. Rev. Genet.* **46**, 69–95 (2012).
- Suzuki, T. in *Fine-Tuning of RNA Functions by Modification and Editing* Vol. 12 (ed. Henri, G.) 23–69 (Springer-Verlag, Berlin-Heidelberg, 2005).
- Nedialkova, D. D. & Leidel, S. A. Optimization of codon translation rates via tRNA modifications maintains proteome integrity. *Cell* **161**, 1606–1618 (2015).
- Suzuki, T., Nagao, A. & Suzuki, T. Human mitochondrial tRNAs: biogenesis, function, structural aspects, and diseases. *Annu. Rev. Genet.* **45**, 299–329 (2011).
- Suzuki, T., Nagano, T. & Suzuki, T. Human mitochondrial diseases caused by lack of taurine modification in mitochondrial tRNAs. *Wiley Interdiscip. Rev. RNA* **2**, 376–386 (2011).
- Suzuki, T. & Suzuki, T. A complete landscape of post-transcriptional modifications in mammalian mitochondrial tRNAs. *Nucleic Acids Res.* **42**, 7346–7357 (2014).
- Suzuki, T., Suzuki, T., Wada, T., Saigo, K. & Watanabe, K. Taurine as a constituent of mitochondrial tRNAs: new insights into the functions of taurine and human mitochondrial diseases. *EMBO J.* **21**, 6581–6589 (2002).
- Kirino, Y., Goto, Y., Campos, Y., Arenas, J. & Suzuki, T. Specific correlation between the wobble modification deficiency in mutant tRNAs and the clinical features of a human mitochondrial disease. *Proc. Natl Acad. Sci. USA* **102**, 7127–7132 (2005).
- Yasukawa, T. et al. A pathogenic point mutation reduces stability of mitochondrial mutant tRNA(Ile). *Nucleic Acids Res.* **28**, 3779–3784 (2000).
- Yasukawa, T., Suzuki, T., Ishii, N., Ohta, S. & Watanabe, K. Wobble modification defect in tRNA disturbs codon-anticodon interaction in a mitochondrial disease. *EMBO J.* **20**, 4794–4802 (2001).
- Kirino, Y. et al. Codon-specific translational defect caused by a wobble modification deficiency in mutant tRNA from a human mitochondrial disease. *Proc. Natl Acad. Sci. USA* **101**, 15070–15075 (2004).
- Fakrudin, M. et al. Defective mitochondrial tRNA taurine modification activates global proteostress and leads to mitochondrial disease. *Cell Rep.* **22**, 482–496 (2018).
- Asano, K. et al. Metabolic and chemical regulation of tRNA modification associated with taurine deficiency and human disease. *Nucleic Acids Res.* **46**, 1565–1583 (2018).
- Umeda, N. et al. Mitochondria-specific RNA-modifying enzymes responsible for the biosynthesis of the wobble base in mitochondrial tRNAs. Implications for the molecular pathogenesis of human mitochondrial diseases. *J. Biol. Chem.* **280**, 1613–1624 (2005).
- Ghezzi, D. et al. Mutations of the mitochondrial-tRNA modifier MTO1 cause hypertrophic cardiomyopathy and lactic acidosis. *Am. J. Hum. Genet.* **90**, 1079–1087 (2012).

19. Kopajtich, R. et al. Mutations in GTPBP3 cause a mitochondrial translation defect associated with hypertrophic cardiomyopathy, lactic acidosis, and encephalopathy. *Am. J. Hum. Genet.* **95**, 708–720 (2014).
20. Guan, M. X. et al. Mutation in TRMU related to transfer RNA modification modulates the phenotypic expression of the deafness-associated mitochondrial 12S ribosomal RNA mutations. *Am. J. Hum. Genet.* **79**, 291–302 (2006).
21. Zeharia, A. et al. Acute infantile liver failure due to mutations in the TRMU gene. *Am. J. Hum. Genet.* **85**, 401–407 (2009).
22. Miyauchi, K., Kimura, S. & Suzuki, T. A cyclic form of N⁶-threonylcarbamoyladenine as a widely distributed tRNA hypermodification. *Nat. Chem. Biol.* **9**, 105–111 (2013).
23. Kimura, S. et al. Discovery of the beta-barrel-type RNA methyltransferase responsible for N⁶-methylation of N⁶-threonylcarbamoyladenine in tRNAs. *Nucleic Acids Res.* **42**, 9350–9365 (2014).
24. Arragain, S. et al. Identification of eukaryotic and prokaryotic methylthiotransferase for biosynthesis of 2-methylthio-N⁶-threonylcarbamoyladenine in tRNA. *J. Biol. Chem.* **285**, 28425–28433 (2010).
25. Matuszewski, M. et al. A hydantoin isoform of cyclic N⁶-threonylcarbamoyladenine (ct⁶A) is present in tRNAs. *Nucleic Acids Res.* **45**, 2137–2149 (2017).
26. Kang, B. et al. Identification of 2-methylthio cyclic N⁶-threonylcarbamoyladenine (ms²ct⁶A) as a novel RNA modification at position 37 of tRNAs. *Nucleic Acids Res.* **45**, 2124–2136 (2017).
27. Murphy, F. V. T., Ramakrishnan, V., Malkiewicz, A. & Agris, P. F. The role of modifications in codon discrimination by tRNA(Lys)UUU. *Nat. Struct. Mol. Biol.* **11**, 1186–1191 (2004).
28. Phelps, S. S., Malkiewicz, A., Agris, P. F. & Joseph, S. Modified nucleotides in tRNA(Lys) and tRNA(Val) are important for translocation. *J. Mol. Biol.* **338**, 439–444 (2004).
29. Niimi, T. et al. Recognition of the anticodon loop of tRNA^{Leu1} by isoleucyl-transfer-RNA synthetase from *Escherichia coli*. *Nucleosides Nucleotides* **13**, 1231–1237 (1994).
30. Lin, C. A., Ellis, S. R. & True, H. L. The Sua5 protein is essential for normal translational regulation in yeast. *Mol. Cell. Biol.* **30**, 354–363 (2010).
31. Deutsch, C., El Yacoubi, B., de Crécy-Lagard, V. & Iwata-Reuyl, D. Biosynthesis of threonylcarbamoyl adenine (t⁶A), a universal tRNA nucleoside. *J. Biol. Chem.* **287**, 13666–13673 (2012).
32. Lauhon, C. T. Mechanism of N⁶-threonylcarbamoyladenine (t⁶A) biosynthesis: isolation and characterization of the intermediate threonylcarbamoyl-AMP. *Biochemistry* **51**, 8950–8963 (2012).
33. Zhang, W., Collinet, B., Perrochia, L., Durand, D. & van Tilbeurgh, H. The ATP-mediated formation of the YgjD-YeaZ-YjeE complex is required for the biosynthesis of tRNA t⁶A in *Escherichia coli*. *Nucleic Acids Res.* **43**, 1804–1817 (2015).
34. Srinivasan, M. et al. The highly conserved KEOPS/EKC complex is essential for a universal tRNA modification, t⁶A. *EMBO J.* **30**, 873–881 (2011).
35. El Yacoubi, B. et al. A role for the universal Kae1/Qri7/YgjD (COG0533) family in tRNA modification. *EMBO J.* **30**, 882–893 (2011).
36. Perrochia, L., Guetta, D., Hecker, A., Forterre, P. & Basta, T. Functional assignment of KEOPS/EKC complex subunits in the biosynthesis of the universal t⁶A tRNA modification. *Nucleic Acids Res.* **41**, 9484–9499 (2013).
37. Edvardson, S. et al. tRNA N⁶-adenosine threonylcarbamoyltransferase defect due to KAE1/TCS3 (OSGEP) mutation manifest by neurodegeneration and renal tubulopathy. *Eur. J. Hum. Genet.* **25**, 545–551 (2017).
38. Braun, D. A. et al. Mutations in KEOPS-complex genes cause nephrotic syndrome with primary microcephaly. *Nat. Genet.* **49**, 1529–1538 (2017).
39. Oberto, J. et al. Qri7/OSGEP, the mitochondrial version of the universal Kae1/YgjD protein, is essential for mitochondrial genome maintenance. *Nucleic Acids Res.* **37**, 5343–5352 (2009).
40. Wan, L. C. et al. Reconstitution and characterization of eukaryotic N⁶-threonylcarbamoylation of tRNA using a minimal enzyme system. *Nucleic Acids Res.* **41**, 6332–6346 (2013).
41. Haussuehl, K. et al. Eukaryotic GCP1 is a conserved mitochondrial protein required for progression of embryo development beyond the globular stage in *Arabidopsis thaliana*. *Biochem. J.* **423**, 333–341 (2009).
42. Horton, P. et al. WoLF PSORT: protein localization predictor. *Nucleic Acids Res.* **35**, W585–W587 (2007).
43. Gakh, O., Cavadini, P. & Isaya, G. Mitochondrial processing peptidases. *Biochim. Biophys. Acta* **1592**, 63–77 (2002).
44. Miyauchi, K., Ohara, T. & Suzuki, T. Automated parallel isolation of multiple species of non-coding RNAs by the reciprocal circulating chromatography method. *Nucleic Acids Res.* **35**, e24–e24 (2007).
45. Suzuki, T., Ikeuchi, Y., Noma, A., Suzuki, T. & Sakaguchi, Y. Mass spectrometric identification and characterization of RNA-modifying enzymes. *Methods Enzymol.* **425**, 211–229 (2007).
46. Bannai, H., Tamada, Y., Maruyama, O., Nakai, K. & Miyano, S. Extensive feature detection of N-terminal protein sorting signals. *Bioinformatics* **18**, 298–305 (2002).
47. Robinson, B. H., Petrova-Benedict, R., Buncic, J. R. & Wallace, D. C. Nonviability of cells with oxidative defects in galactose medium: a screening test for affected patient fibroblasts. *Biochem. Med. Metab. Biol.* **48**, 122–126 (1992).
48. Cox, R. et al. Leigh syndrome caused by a novel m.4296G A mutation in mitochondrial tRNA isoleucine. *Mitochondrion* **12**, 258–261 (2012).
49. Smith, D. G., Pal, R. & Parker, D. Measuring equilibrium bicarbonate concentrations directly in cellular mitochondria and in human serum using europium/terbium emission intensity ratios. *Chemistry* **18**, 11604–11613 (2012).
50. Wilson, W. R. & Hay, M. P. Targeting hypoxia in cancer therapy. *Nat. Rev. Cancer* **11**, 393–410 (2011).
51. Thiaville, P. C. et al. Cross kingdom functional conservation of the core universally conserved threonylcarbamoyladenine tRNA synthesis enzymes. *Eukaryot. Cell* **13**, 1222–1231 (2014).
52. Nakano, S., Suzuki, T., Kawarada, L., Iwata, H. & Asano, K. NSUN3 methylase initiates 5-formylcytidine biogenesis in human mitochondrial tRNA(Met). *Nat. Chem. Biol.* **12**, 546–551 (2016).
53. Cui, H. et al. Comprehensive next-generation sequence analyses of the entire mitochondrial genome reveal new insights into the molecular diagnosis of mitochondrial DNA disorders. *Genet. Med.* **15**, 388–394 (2013).
54. Martikainen, M. H., Kytovuori, L. & Majamaa, K. Juvenile parkinsonism, hypogonadism and Leigh-like MRI changes in a patient with m.4296G A mutation in mitochondrial DNA. *Mitochondrion* **13**, 83–86 (2013).
55. Juhling, F. et al. tRNAdb 2009: compilation of tRNA sequences and tRNA genes. *Nucleic Acids Res.* **37**, D159–D162 (2009).
56. Yamamoto, Y., Hasegawa, J. & Ito, Y. Kinetic investigation on carbamate formation from the reaction of carbon dioxide with amino acids in homogeneous aqueous solution. *J. Phys. Org. Chem.* **25**, 239–247 (2012).
57. Geyer, R. P. & Chang, R. S. Bicarbonate as an essential for human cells in vitro. *Arch. Biochem. Biophys.* **73**, 500–506 (1958).
58. Harris, A. L. Hypoxia—a key regulatory factor in tumour growth. *Nat. Rev. Cancer* **2**, 38–47 (2002).
59. Denko, N. C. Hypoxia, HIF1 and glucose metabolism in the solid tumour. *Nat. Rev. Cancer* **8**, 705–713 (2008).
60. Semenza, G. L. Targeting HIF-1 for cancer therapy. *Nat. Rev. Cancer* **3**, 721–732 (2003).
61. Benej, M., Pastorekova, S. & Pastorek, J. Carbonic anhydrase IX: regulation and role in cancer. *Subcell. Biochem.* **75**, 199–219 (2014).
62. Vander Heiden, M. G., Cantley, L. C. & Thompson, C. B. Understanding the Warburg effect: the metabolic requirements of cell proliferation. *Science* **324**, 1029–1033 (2009).
63. Pyzocha, N. K., Ran, F. A., Hsu, P. D. & Zhang, F. RNA-guided genome editing of mammalian cells. *Methods Mol. Biol.* **1114**, 269–277 (2014).
64. Cong, L. et al. Multiplex genome engineering using CRISPR/Cas systems. *Science* **339**, 819–823 (2013).
65. Varshney, U., Lee, C. P. & RajBhandary, U. L. Direct analysis of aminoacylation levels of tRNAs in vivo. Application to studying recognition of *Escherichia coli* initiator tRNA mutants by glutamyl-tRNA synthetase. *J. Biol. Chem.* **266**, 24712–24718 (1991).
66. Arai, T., Ishiguro, K., Kimura, S., Sakaguchi, Y. & Suzuki, T. Single methylation of 23S rRNA triggers late steps of 50S ribosomal subunit assembly. *Proc. Natl Acad. Sci. USA* **112**, E4707–E4716 (2015).
67. Sampson, J. R. & Uhlenbeck, O. C. Biochemical and physical characterization of an unmodified yeast phenylalanine transfer RNA transcribed in vitro. *Proc. Natl Acad. Sci. USA* **85**, 1033–1037 (1988).
68. Trounce, I. A., Kim, Y. L., Jun, A. S. & Wallace, D. C. Assessment of mitochondrial oxidative phosphorylation in patient muscle biopsies, lymphoblasts, and transmittochondrial cell lines. *Methods Enzymol.* **264**, 484–509 (1996).
69. Leary, S. C. & Sasarman, F. Oxidative phosphorylation: synthesis of mitochondrially encoded proteins and assembly of individual structural subunits into functional holoenzyme complexes. *Methods Mol. Biol.* **554**, 143–162 (2009).
70. Ruiz-Pesini, E. et al. An enhanced MITOMAP with a global mtDNA mutational phylogeny. *Nucleic Acids Res.* **35**, D823–D828 (2007).

Acknowledgements

We are grateful to the Suzuki laboratory members, especially to Takeo Suzuki, and Asutaka Nagao for many fruitful discussions and technical advices. This work was supported by Grants-in-Aid for Scientific Research on Priority Areas from the Ministry

of Education, Science, Sports, and Culture of Japan (T.S.), and Grants-in-Aid of the Research on Intractable Diseases (Mitochondrial Disorder) from the Ministry of Health, Labour and Welfare of Japan (Y.G.).

Author contributions

H.L. mainly performed the series of experiments. K.M., T.H., R.O., and Y.S. assisted in the biochemical works. E.T., H.K., K.F., H.Y., and Y.G. established and cultured the patient cells. K.Y. and S.N. supported the animal experiments. All authors discussed the results. T.S. and H.L. wrote this paper. T.S. designed and supervised all the work.

Additional information

Supplementary Information accompanies this paper at <https://doi.org/10.1038/s41467-018-04250-4>.

Competing interests: The authors declare no competing interests.

Reprints and permission information is available online at <http://npg.nature.com/reprintsandpermissions/>

Publisher's note: Springer Nature remains neutral with regard to jurisdictional claims in published maps and institutional affiliations.



Open Access This article is licensed under a Creative Commons Attribution 4.0 International License, which permits use, sharing, adaptation, distribution and reproduction in any medium or format, as long as you give appropriate credit to the original author(s) and the source, provide a link to the Creative Commons license, and indicate if changes were made. The images or other third party material in this article are included in the article's Creative Commons license, unless indicated otherwise in a credit line to the material. If material is not included in the article's Creative Commons license and your intended use is not permitted by statutory regulation or exceeds the permitted use, you will need to obtain permission directly from the copyright holder. To view a copy of this license, visit <http://creativecommons.org/licenses/by/4.0/>.

© The Author(s) 2018